Latent heat flux and canopy conductance based on Penman-Monteith and Bouchet's complementary hypothesis

validation over diverse biomes

Mallick, K; Jarvis, A; Tu, K; Fischer, J.; Boegh, Eva; Niyogi, D

Published in:
Journal of Hydrometeorology

DOI:
10.1175/JHM-D-12-0117.1

Publication date:
2013

Document Version
Publisher's PDF, also known as Version of record

Citation for published version (APA):
Mallick, K., Jarvis, A., Tu, K., Fischer, J., Boegh, E., & Niyogi, D. (2013). Latent heat flux and canopy conductance based on Penman-Monteith and Bouchet's complementary hypothesis: validation over diverse biomes. *Journal of Hydrometeorology*, *14*(2), 419-442. https://doi.org/10.1175/JHM-D-12-0117.1

Latent Heat Flux and Canopy Conductance Based on Penman–Monteith, Priestley–Taylor Equation, and Bouchet's Complementary Hypothesis

KANISKA MALLICK,* ANDREW JARVIS,+ JOSHUA B. FISHER,* KEVIN P. TU,# EVA BOEGH,@ AND DEV NIYOGI&

* *Jet Propulsion Laboratory, California Institute of Technology, Pasadena, California*
+ *Lancaster Environment Centre, Lancaster University, Lancaster, United Kingdom*
# *Pioneer Hi-Bred International, Woodland, California*
@ *Department of Environmental Social and Spatial Change, Roskilde University, Roskilde, Denmark*
& *Department of Agronomy, and Department of Earth and Atmospheric and Planetary Sciences, Purdue University, West Lafayette, Indiana*

(Manuscript received 9 August 2012, in final form 2 November 2012)

ABSTRACT

A novel method is presented to analytically resolve the terrestrial latent heat flux (λE) and conductances (boundary layer g_B and surface g_S) using net radiation (R_N), ground heat flux (G), air temperature (T_a), and relative humidity (RH). This method consists of set of equations where the two unknown internal state variables (g_B and g_S) were expressed in terms of the known core variables, combining diffusion equations, the Penman–Monteith equation, the Priestley–Taylor equation, and Bouchet's complementary hypothesis. Estimated λE is validated with the independent eddy covariance λE observations over Soil Moisture Experiment 2002 (SMEX-02); the Global Energy and Water Cycle Experiment (GEWEX) Continental-Scale International Project (GCIP) selected sites from FLUXNET and tropics eddy flux, representing four climate zones (tropics, subtropics, temperate, and cold); and multiple biomes. The authors find a RMSE of 23.8–54.6 W m^{-2} for hourly λE over SMEX-02 and GCIP and 23.8–29.0 W m^{-2} for monthly λE over the FLUXNET and tropics. Observational and modeled evidence in the reduction in annual evaporation (E) pattern on the order of 33% from 1999 to 2006 was found in central Amazonia. Retrieved g_S responded to vapor pressure deficit, measured λE, and gross photosynthesis in a theoretically robust behavior. However, the current scheme [Penman–Monteith–Bouchet–Lhomme (PMBL)] showed some overestimation of λE in limited soil moisture regimes. PMBL provides similar results when compared with another Priestley–Taylor–based λE estimation approach [Priestley–Taylor–Jet Propulsion Laboratory (PT-JPL)] but with the advantage of having the conductances analytically recovered.

1. Introduction

Accurate surface energy balance is an important integral objective of the land surface model (LSM) and hydrology schemes embedded within the climate and Earth system models. Central to the surface energy balance is the latent heat flux (λE) (or evaporation E) that drives the global atmospheric circulation (Numaguti 1993; Trenberth et al. 2002), contributes significant variability (Lohmann et al. 1998; Werth and Avissar 2004) in the global hydrological cycle, and is identified as an essential climate variable. Some recent studies have demonstrated significant disagreement among climate models, attributed mainly to the differences in the LSMs associated with them, and λE has been identified as one of the important land surface process variables where major attention is needed (Pitman 2003).

To date, the methods for estimating λE and its internal state variables (canopy conductance g_S and boundary layer conductance g_B) have been largely based on unidimensional computational models having various LSMs in their core (Bonan 1995; Foley et al. 1996; Sellers et al. 1997; Niyogi and Raman 1997). While λE estimates from the LSM forward runs are commonly compared with the eddy covariance (EC) data, those models are generally calibrated over some specific sites,

Corresponding author address: K. Mallick, Jet Propulsion Laboratory, California Institute of Technology, 4800 Oak Grove Dr., Pasadena, CA 91109.
E-mail: kaniska.mallick@gmail.com

DOI: 10.1175/JHM-D-12-0117.1

and their independent global evaluation on other sites produces significant uncertainty (Bonan 2008).

The Penman–Monteith equation (PME; Penman 1948; Monteith 1965) is the most widely accepted method for estimating λE from the terrestrial surfaces (Sumner and Jacobs 2005). The main advantage of the PME is that it does not require any surface temperature information. However, the disadvantage of PME is that, unlike the standard meteorological variables, the boundary layer conductance (g_B) and the canopy (or stomatal) conductance (g_S) are not available as paired observations. Therefore, PME requires information about the surface roughness and atmospheric stability–instability conditions to estimate both g_B and g_S. Measuring g_S at the leaf level and integration for the whole canopy is difficult and uncertain, while modeling g_S is error prone because plant physiological processes are controlled both by the physical environment and by the strategic behavior of plants for their optimal functioning (Katul et al. 2010). Although it would be possible to assume a mechanistic (Leuning 1995), empirical (Jarvis 1976), or semi-empirical model (Ball et al. 1987) for g_S, unlike λE, no universally agreed predictors for g_S have been identified. All the commonly used g_S models were originally derived from direct measurements of g_S in controlled laboratory environments. These environments do not necessarily capture spatiotemporal heterogeneity of the atmospheric and land surface states. Furthermore, these models were developed based on data collected from leaf-level measurements. For hydrological applications and LSMs, canopy-level g_S is required. The complex structure of canopies, heterogeneity of leaf physiological features, and variations within canopy microclimate make g_S significantly variable among the plant leaves. This makes it difficult to accurately derive the lumped canopy-scale g_S values from the leaf-level measurements. Upscaling of leaf-to-canopy g_S involves substantial simplifications and assumptions that could lead to large uncertainties.

Specification of g_B is equally complicated because of differences in the boundary layer conductance between the surface and the air and the boundary layer conductance between the canopy source height and the air above the canopy (Troufleau et al. 1997). This difference is empirically adjusted through introducing an ''excess'' conductance between the canopy source height and the surface (Troufleau et al. 1997), which, in the heterogeneous surface condition, is a complex function of canopy geometry and wind profile structure within the canopy. Estimating g_B through such an approach involves a significant amount of empiricism to specify the surface roughness lengths, displacement height, and stability–instability criteria (Thom 1975; Choudhury et al. 1986; Troufleau et al. 1997), which are not time and space invariant. While the parameterized g_B has been used with modest success, large-scale application is still highly uncertain. Given the reasons described above, an alternative, therefore, may be to analytically recover g_B and g_S from the data itself and then try to estimate λE. Boegh et al. (2002) and Boegh and Soegaard (2004) had demonstrated an approach while estimating λE and conductances using remote sensing data that highlights the possibilities of resolving surface energy balance nonparametrically.

In this study, we describe a method for retrieving g_B and g_S using a semi-nonparametric approach followed by the estimation of λE. The method centers on combining the Penman–Monteith equation (Penman 1948; Monteith 1965), the Priestley–Taylor equation (Priestley and Taylor 1972) and Bouchet's (Bouchet 1963) complementary hypothesis in conjugation with the diffusion equations of scalar transfer. It only requires inputs of net radiation (R_N), ground heat flux (G), air temperature (T_a), and relative humidity (RH) or vapor pressure (e_a). An inherent advantage is that no calibration or spinup is needed, so the method has spatiotemporal scalability (from hourly to annual and landscape to globe).

The objectives of the paper are 1) to develop a semi-nonparametric λE estimation method based on combining the Penman–Monteith and Priestley–Taylor equations with diffusion equations and Bouchet's complementary hypothesis, 2) to assess the ability of the scheme to capture the temporal variability of λE over different agricultural and forest ecosystems in different climate zones using atmospheric eddy covariance data, and 3) to evaluate the retrieved canopy conductance.

In this study, a range of radiation, meteorological and surface flux datasets from diverse climate zones covering multiple biome types are compiled and used. These include half-hourly data from international experiments [e.g., Soil Moisture Experiment 2002 (SMEX-02; Prueger et al. 2005) and the Global Energy and Water Cycle Experiment (GEWEX) Continental-Scale International Project (GCIP; National Research Council 1998)] and monthly data from FLUXNET and related eddy covariance tower sites (Baldocchi et al. 2001). While retrieving g_B and g_S, we also retrieved four additional variables: vapor pressure of the evaporating front (e_s), saturation vapor pressure of the evaporating front (e_S^*), evaporative fraction (EF), and aerodynamic and air temperature difference (dT). Section 2 describes the derivation of expressions for all six variables. Section 3 describes the sensitivity analysis methodology, while the description of the datasets is given in section 4. The validation of λE and the analysis of the retrieved g_S is detailed in section 5. Study results are discussed in

TABLE 1. List of variable retrieved and the equations used in the study.

Unknown variables	Name	Equation	Inputs
g_B	Boundary layer conductance	$g_B = \dfrac{\Phi}{\rho C_p\left[dT + \dfrac{e_S - e_a}{\gamma}\right]}$	R_N, G, T_a, and RH
g_S	Canopy conductance	$g_S = Mg_B\dfrac{e_S^* - e_a}{e_S^* - e_S}$	
e_S	Actual vapor pressure of the evaporating front	$e_S = e_a + M(e_S^* - e_a)$	
dT	Aerodynamic and air temperature difference	$dT = \left(\dfrac{e_S - e_a}{\gamma}\right)\left(\dfrac{1-\text{EF}}{\text{EF}}\right)$	
e_S^*	Saturation vapor pressure of the evaporating front	$e_S^* = e_a^* + \Delta dT$	
EF	Evaporative fraction	$\text{EF} = \dfrac{k\alpha\Delta}{2\Delta + \gamma\left(2 + \dfrac{g_B}{g_S}\right)}$	

section 6, and the strengths and limitations of the proposed approach are outlined in section 7.

2. Methodology

The proposed method seeks to analytically solve g_B and g_S. In deriving the expressions for g_B and g_S, we have also introduced four more unknown variables (e_S, e_S^*, EF, and dT). The core equations are given in Table 1, and their detailed derivation is explained below.

a. Expression for g_B

The surface energy balance equation is written as

$$\Phi = H + \lambda E, \tag{1}$$

where Φ is net available energy ($\cong R_N - G$), H is sensible heat flux, λE is latent heat flux, R_N is net radiation, and G is conductive surface heat flux or ground heat flux. All the fluxes are in watts per meter squared:

$$H = \rho C_P g_B dT, \tag{2}$$

$$\lambda E = \frac{\rho C_P}{\gamma} g_B (e_S - e_a), \tag{3}$$

where ρ is air density (kg m^{-3}), C_P is specific heat of dry air (MJ kg^{-1} K^{-1}), γ is the psychrometric constant (hPa K^{-1}), dT is the difference between the aerodynamic temperature (T_{aero}, temperature at canopy source height) and air temperature T_a (K), and e_S is the actual vapor pressure (hPa) of the evaporating front where T_{aero} is satisfied. T_{aero} is the temperature of the thin boundary layer in the immediate vicinity of the surface level and is responsible for the transfer of heat from the surface to the atmosphere. Generally, dT is expressed as the difference between the radiometric surface temperature (T_{sfc}) and the air temperature (T_a), but T_{sfc} is not the true temperature that is responsible for transferring the sensible heat flux (Troufleau et al. 1997). In spite of the apparent simplicity of Eq. (2), the main limitation lies in the definition of surface temperature. Considering the vertical extension of vegetation or canopy, the concept of ''surface'' and its associated level is quite confusing (Norman and Campbell 1998). Equation (2) is specially inferred from the aerodynamic transfer equations, which means that T_{sfc} is theoretically an air temperature at the surface, which is different from the physical temperature of the surface (Monteith 1965). The level that satisfies T_{aero} is defined as the source height where wind speed is zero and T_{aero} is obtained by extrapolating the logarithmic profile of T_a down to that level. Stewart and Thom (1973) postulated that the effective source of sensible heat flux is located at a lower level that the effective sink of momentum. Hence, dT is equivalent to the difference between T_{aero} and T_a and is treated as an unknown state variable in the present study. By combining Eqs. (1), (2), and (3) and expressing for g_B, we get

$$g_B = \frac{\Phi}{\rho C_P\left[dT + \dfrac{(e_S - e_a)}{\gamma}\right]}. \tag{4}$$

b. Expression for g_S

An equation of canopy (or stomatal) conductance (g_S) is obtained from the following diffusion equation expression. According to the diffusion equation, λE can be also expressed as

$$\lambda E = \frac{\rho C_P}{\gamma} g_S (e_S^* - e_S) \tag{5}$$

and

$$\lambda E = M \times \text{PE} = M\frac{\rho C_P}{\gamma} g_B (e_S^* - e_a), \tag{6}$$

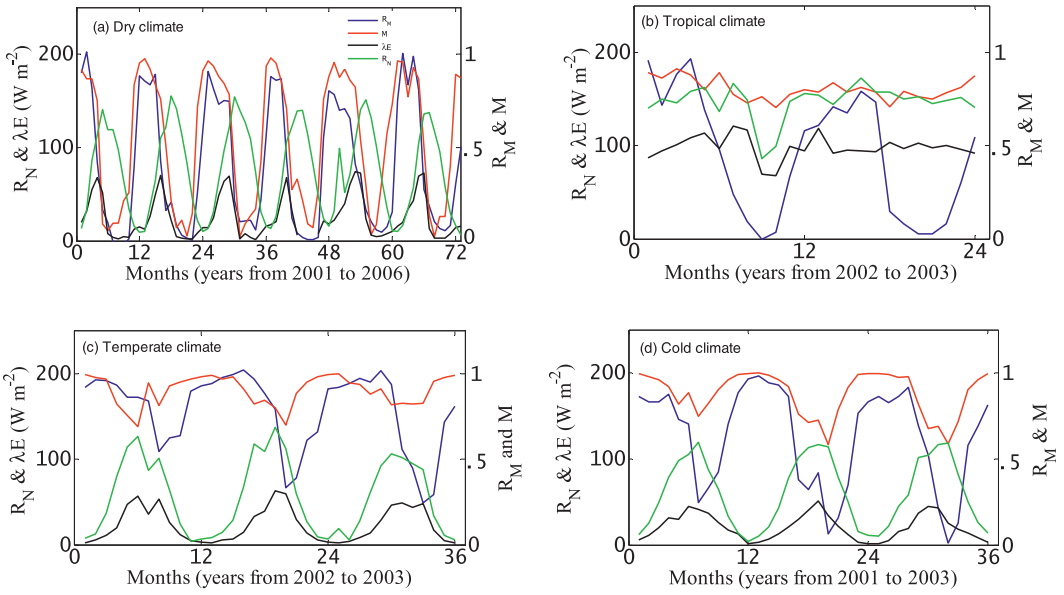

FIG. 1. Temporal patterns of M (=$\mathrm{RH}^{\mathrm{VPD}}$) ($f_{\mathrm{SM}}$ in Fisher et al. 2008) and relative surface moisture (R_M) along with the R_N and λE over the (a)–(d) four prime climates (according to Köppen's classification) of the world. These are the observational data from the FLUXNET eddy covariance network, where representative sites falling under the individual climate regions are exemplified. This clearly shows the strong control of moisture on λE in the dry climate and little control of moisture in the temperate and cold climate. These figures also reveal the control of radiation on λE in the temperate and cold climate, whereas in the tropical and subtropical dry climate both moisture and radiation impose strong controls on λE.

where e_S^* is saturation vapor pressure (hPa) of the evaporating front and M is the limiting factor that is responsible for constraining potential evaporation (PE) into λE. Equation (6) resembles the α–β formulations of λE (Noilhan and Planton 1989; Lee and Pielke 1992; Cahill et al. 1999). From Eqs. (5) and (6), we can express g_S in terms of g_B, e_S^*, e_s, e_a^*, e_a, and M:

$$g_S = M \times g_B \frac{e_S^* - e_a}{e_S^* - e_S}. \tag{7}$$

For the vegetation, water vapor transfer occurs from within the vegetation (transpiration) and from the immediate vicinity of the vegetation surface (evaporation). For dense canopies and moist soils, T_{sfc} may approach the true aerodynamic temperature of the evaporating surface (Lhomme et al. 2000). The stomatal cavities can be assumed to be saturated; therefore, e_S^* of dense canopies can always be estimated from T_{sfc}. But for extremely dry, bare soil, the evaporating front is located much below the dry surface layer of different thermal property, and the true T_{sfc} may be different than the surface T_{sfc} by a few degrees. Despite the availability of T_{sfc} data from the current generation of polar orbiting satellites, T_{sfc} is not used in the present study because of the differences between the physical versus aerodynamic temperature, as described above. Therefore, e_S^* was treated as an unknown variable and expressed according to Monteith (1965) [Eq. (14) and Table 1].

We hypothesize M to be a stress factor that arises because of moisture or wetness availability (or unavailability). A wide range of M can be found in the natural ecosystems in different climatic regions of the world. The tropical region has little variability in M, whereas the dry climate (covering the Mediterranean savanna and arid–semiarid region) has an extremely large variability in M (Fig. 1). Series of research have already expressed M as a function of soil moisture, soil water potential, and atmospheric vapor pressure deficit (VPD; Noilhan and Planton 1989; Kondo et al. 1990).

Fisher et al. (2008) expressed $M = \mathrm{RH}^{\mathrm{VPD}}$ (RH in a fraction and VPD in kilopascals; equivalent to f_{SM} in Fisher et al. 2008) and found that this is equivalent to the relative extractable surface moisture (R_M). The hypothesis was that the surface soil moisture (and, hence, extractable near-surface soil moisture) could be inferred from the atmospheric moisture and that there is no resistance to transfer between them that will ultimately prevent them from reaching equilibrium. Atmospheric resistance only delays the process of equilibration but does not prevent it, if given enough time. In contrast, plants can actively maintain disequilibrium from the

atmosphere via stomatal closure. Under the conditions when $M = 0$ and the surface soil moisture is 0, the plants may access groundwater via deep roots that extend below the surface soil layers. This would be consistent with the occurrence of transpiration in very dry environments where $\mathrm{RH} \rightarrow 0$ but there is still sparse green vegetation. Therefore, the difference between e_S and e_a is very small when $\mathrm{RH} \rightarrow 0$. Such conditions exist in the dry climate (arid–semiarid, savanna, temperate, and cold) where atmospheric moisture demand remains high and the vertical column from surface to subsurface is also extremely dry. On the contrary, under the influence of high RH and low atmospheric water demand (tropics, wet temperate, and wet cold climate), M tends to be high and does not impose any strong constraint on g_S and λE. Vegetation transpires at the optimum rate mainly under the influence of available energy under such conditions. The characteristic pattern of M across different climates is shown in Figs. 1a–d and is calculated following the Fisher et al. (2008) equation.

The soil moisture data from active–passive microwave sensors (e.g., QuikSCAT, AMSR-E, and SMOS) can be used, but the soil moisture estimates from these current microwave satellite sensors are prone to large uncertainties, especially in the densely vegetated landscapes (Mallick et al. 2009).

In Eqs. (4) and (7), there are five unknowns: g_B, g_S, dT,e_S^*, and e_S. We need to identify other equations to solve for the other three unknowns (e_S, dT, and e_S^*).

c. *Expression for e_S*

While rewriting the Penman–Monteith equation, the vapor pressure deficit at the evaporating front was given by Jarvis and McNaughton (1986) as follows:

$$e_S^* - e_S = \Omega(e_S^* - e_S)_{\mathrm{eq}} + (1 - \Omega)\mathrm{VPD}, \tag{8}$$

where $\Omega = (\Delta/\gamma + 1)/(\Delta/\gamma + 1 + g_B/g_S)$ is the decoupling coefficient, which quantifies the degree of coupling between the surface and the overlying atmosphere; $(e_S^* - e_S)_{\mathrm{eq}}$ is the equilibrium surface vapor pressure deficit (hPa); and Δ is the slope of the saturation vapor pressure versus air temperature (hPa K^{-1}). Under efficient vertical mixing of the air, g_B increases and $\Omega \rightarrow 0$, which implies a good surface–atmosphere coupling. According to Eq. (8), when the surface is fully coupled to the atmosphere ($\Omega = 0$), the VPD is imposed at the surface. On the contrary, when the surface is completely decoupled from the atmosphere ($\Omega = 1$), the surface vapor pressure deficit in that condition can be solved as $(e_S^* - e_S)_{\mathrm{eq}} = (\lambda E_{\mathrm{eq}}/g_S)(\gamma/\rho C_P)$, where λE_{eq} is the equilibrium latent heat flux given as $\lambda E_{\mathrm{eq}} = \Phi(\Delta/\Delta + \gamma)$ (Jarvis and McNaughton 1986). When the surface–air temperature difference increases above 10°C, the linear approximation of Δ in the Penman–Monteith equation becomes invalid (Paw U and Gao 1988). Dry bare soil very often attains this temperature difference in many parts of the world during summer. Under the decoupled condition, using nonlinear solutions for the saturated vapor pressure results the limit of λE to approach the net available energy (Φ), which may be very different from the λE_{eq} used to calculate $(e_S^* - e_S)_{\mathrm{eq}}$ (Paw U and Gao 1988). Therefore, the application of Eq. (8) for evaluation of e_s may produce a significant error when g_B/g_S approaches a big value (i.e., when $g_B/g_S \rightarrow \infty$).

For the prediction of e_S, the decoupling coefficient (Ω) was used to quantify the degree of coupling between the surface and the atmosphere (Jarvis and McNaughton 1986). When the surface and the atmosphere are tightly coupled ($\Omega \rightarrow 0$), e_S approaches e_a, and when the surface is fully decoupled from the atmosphere ($\Omega \rightarrow 1$), water vapor starts accumulating at the surface and e_S approaches e_S^*. The limit of e_S during decoupled conditions may be calculated from the T_{sfc} measurement. Earlier, Boegh et al. (2002) and Boegh and Soegaard (2004) investigated the feasibility of using Ω as an empirical weighting factor to place e_s between its limit values, e_S^* and e_a, by using the following two equations:

$$e_S = \Omega h_{S_{\max}} e_S^* + (1 - \Omega)e_a, \tag{9a}$$

$$e_S = \Omega \Lambda e_S^* + (1 - \Omega)e_a, \tag{9b}$$

where $h_{S_{\max}}$ is the maximum upper level for the relative air humidity at the surface, which was parameterized empirically with fractional vegetation cover and Λ is an adjustment factor (humidity related) analytically related to the vapor pressure and conductances. A constant value of Λ (=0.9) was assigned to compute evapotranspiration for a wide range of surface conditions. Looking at the description of both $h_{S_{\max}}$ and Λ, the surface humidity is not necessarily dependent on fractional vegetation cover, but it is dependent on surface moisture availability (M) or surface humidity (Lee and Pielke 1992). Similarly, using Λ as a static value may lead to errors under very dry surface conditions. Instead of using a land cover–dependent moisture variable or a constant moisture variable, we expressed the surface humidity or surface moisture availability according to Fisher et al. (2008), and e_S is expressed as follows:

$$e_S = e_a + M(e_S^* - e_a). \tag{10}$$

This equation is very similar to the expressions used by Nappo (1975), Ye and Pielke (1993), and Wetzel et al. (1984).

d. Expression for dT and e_S^*

After finding an expression of e_S, the next step is to find an expression of dT. Here we used the Bowen ratio (β) equation (Bowen 1926):

$$\beta = \gamma \frac{dT}{e_S - e_a}. \tag{11}$$

With the assumption of surface energy balance closure, β can also be expressed in terms of EF as (Shuttleworth et al. 1989)

$$\beta = \frac{1 - \mathrm{EF}}{\mathrm{EF}}. \tag{12}$$

The quantity EF is defined as the fraction of available energy (Φ) partitioned toward λE. Substituting β in Eq. (11), we can get an expression of dT in terms of EF:

$$dT = \left(\frac{e_S - e_a}{\gamma}\right)\left(\frac{1 - \mathrm{EF}}{\mathrm{EF}}\right). \tag{13}$$

We have expressed e_S^* according to Monteith (1965):

$$e_S^* = e_a^* + \Delta dT. \tag{14}$$

While finding the expression of dT, we have introduced one extra variable, EF. Therefore, to close the system of equations, we need one more equation. The derivation of the expression for EF is described below.

e. Expression for EF

According to the PME (Penman 1948; Monteith 1965),

$$\mathrm{PE_{PM}} = \frac{\Delta\Phi + \rho C_P g_B \mathrm{VPD}}{\Delta + \gamma}, \tag{15}$$

$$\lambda E = \frac{\Delta\Phi + \rho C_P g_B \mathrm{VPD}}{\Delta + \gamma\left(1 + \dfrac{g_B}{g_S}\right)}, \tag{16}$$

where Δ is the slope of the saturation vapor pressure versus air temperature relationship (hPa K^{-1}), Φ is the net available energy driving latent heat (W m^{-2}), ρ is air density (kg m^{-3}), C_P is the specific heat of dry air (MJ kg^{-1} K^{-1}), VPD is the atmospheric vapor pressure deficit (hPa), γ is the psychometric constant (hPa K^{-1}), and $\mathrm{PE_{PM}}$ is the potential evaporation according to Penman. It is defined as the evaporation that would take place from a moist surface under prevailing weather conditions, limited only by the net available energy. Other terms in the above two equations are explained earlier.

Dividing Eq. (16) by Eq. (15), we get

$$\frac{\lambda E}{\mathrm{PE_{PM}}} = \frac{\Delta + \gamma}{\Delta + \gamma\left(1 + \dfrac{g_B}{g_S}\right)}. \tag{17}$$

On regional scales, PE and λE are dependent on each other. Bouchet (1963) first proposed, for a large homogeneous area with minimum advection of heat and moisture, that PE and λE are strongly coupled through a complementary land–atmosphere feedback mechanism. He hypothesized that, under the conditions of constant energy supply to any given surface–atmosphere system, when the water availability becomes limited, λE falls below PE, and some amount of energy becomes available. This extra energy increases the temperature and humidity gradient of the overlying air (in the form of sensible heat or longwave back radiation) and leads to an increase in PE whose magnitude is equal to the decrease in λE. If moisture availability is increased, λE again starts increasing and PE decreases. Under the condition of unlimited moisture supply, λE equals PE is referred to as wet environment evaporation (ET_W). If the energy budget remains unchanged and all the excess energy is converted into the sensible heat flux, a complementary relationship of the form $\lambda E + \mathrm{PE} = k \times \mathrm{ET}_W$ exists, where $k = 2$.

According to the complementary relationship advection aridity hypothesis of Brutsaert and Stricker (1979), ET_W was approximated as the potential evaporation according to Priestley and Taylor (1972) ($\mathrm{PE_{PT}}$) and PE was expressed as the potential evaporation according to Penman (1948) ($\mathrm{PE_{PM}}$). Therefore,

$$\lambda E + \mathrm{PE_{PM}} = k \times \mathrm{ET_{PT}}. \tag{18}$$

From the above expression, ET_W is a constant for a prevailing atmospheric condition and moisture availability. According to traditional Budyko approach (Budyko et al. 1962; Roderick and Farquhar 2004), in case of complementarity, the regional λE is limited by moisture availability in the arid climate and λE is limited by energy availability in the humid climate. However, the complementary relationship allows regional PE to depend on regional λE in a complementary manner throughout any range of moisture and energy availability (Ramirez et al. 2005).

Some theoretical arguments suggest that the hypothesis of 1:1 compensation between λE and PE around ET_W is only partially fulfilled (Lhomme 1997; Sugita

et al. 2001). Lhomme (1997) have shown that k is a function of both g_S and g_B, and k is equal to 2 when $g_S = 0$ (i.e., under the wettest surface condition) or when $g_B \to \infty$ (i.e., k tends to be 2 as the surface appears smooth). Otherwise, the expression of k becomes $k = [2 + 1/(1 + \varepsilon)(g_B/g_S)]/\alpha$. However, very recently Ramirez et al. (2005) found observational evidence of the complementary relationship and confirmed the value of k to be 2 (standard deviation ±0.02). Therefore, we opted for $k = 2$ in the present study; α is the Priestley–Taylor coefficient (1.26) and $\varepsilon = \Delta/(\Delta + \gamma)$. From the above equation,

$$\mathrm{PE_{PM}} = k \times \mathrm{PE_{PT}} - \lambda E. \tag{19}$$

Dividing both sides of Eq. (19) by λE, we get

$$\frac{\lambda E}{\mathrm{PE_{PM}}} = \frac{\lambda E}{k \times \mathrm{PE_{PT}} - \lambda E}. \tag{20}$$

Dividing the numerator and denominator of the right-hand side of Eq. (19) by $\mathrm{PE_{PT}}$, we get

$$\frac{\lambda E}{\mathrm{PE_{PM}}} = \frac{\dfrac{\lambda E}{\mathrm{PE_{PT}}}}{k - \dfrac{\lambda E}{\mathrm{PE_{PT}}}}. \tag{21}$$

According to Priestley and Taylor (1972),

$$\mathrm{PE_{PT}} = \alpha \frac{\Delta}{\Delta + \gamma}\Phi,$$

where Φ can also be expressed as $\Phi = (\lambda E/\mathrm{EF})$. Therefore,

$$\mathrm{PE_{PT}} = \alpha \frac{\Delta}{\Delta + \gamma}\frac{\lambda E}{\mathrm{EF}}$$

$$\frac{\lambda E}{\mathrm{PE_{PT}}} = \frac{\Delta + \gamma}{\alpha\Delta}\mathrm{EF}. \tag{22}$$

Now, substituting this expression of $\lambda E/\mathrm{PE_{PT}}$ from (22) into (21) and after some algebra,

$$\frac{\lambda E}{\mathrm{PE_{PM}}} = \frac{\mathrm{EF}(\Delta + \gamma)}{k\alpha\Delta - \mathrm{EF}(\Delta + \gamma)}. \tag{23}$$

Replacing $\lambda E/\mathrm{PE_{PM}}$ between (17) and (23), we can express EF in terms of conductance:

$$\frac{\mathrm{EF}(\Delta + \gamma)}{k\alpha\Delta - \mathrm{EF}(\Delta + \gamma)} = \frac{\Delta + \gamma}{\Delta + \gamma\left(1 + \dfrac{g_B}{g_S}\right)}$$

After some algebra, the final expression of EF in terms of g_B and g_S is

$$\mathrm{EF} = \frac{k\alpha\Delta}{2\Delta + \gamma\left(2 + \dfrac{g_B}{g_S}\right)}. \tag{24}$$

Now we can solve Eqs. (4), (7), (10), (13), (14), and (24) to retrieve g_B, g_S, dT, e_S, e_S^*, and EF. We name our method Penman–Monteith–Bouchet–Lhomme (PMBL).

3. Sensitivity analysis

Given that the λE outputs from PMBL are dependent on the four core variables, a one-dimensional sensitivity analysis (Sanchez et al. 2009) was carried out to assess the impacts of the propagation of uncertainty of the input variables into the λE estimates. The input variables (T_a, RH, R_N, and G) were changed by ±10% from their reference value range, except for air temperature (T_a), for which ±2-K perturbation was assigned. The method computes the relative sensitivity S of λE to p uncertainties in the individual four variables. The sensitivity is finally expressed as

$$S = \frac{\lambda E_{p+} - \lambda E_{p-}}{\lambda E_r},$$

where λE_r is the estimated value of λE when the value of any of the four variables are at their reference value, λE_{p+} is the estimated value of λE when the value of any of the four variables is increased by p from its reference value without perturbing the other input variables, and λE_{p-} is the estimated value of λE when the value of any of the four variables is decreased by p from its reference value without perturbing the other input variables.

4. Datasets

According to the equations described in Table 1, estimation of λE in PMBL requires information R_N, G, T_a, RH, or e_a. All four variables are available from different international flux measurement experiments, the FLUXNET network, and a tropical forest flux site database compiled by Fisher et al. (2009). An eddy covariance method was used in all cases to quantify the vertical fluxes between the ecosystem and the atmosphere from the covariance between vertical wind velocity and scalar fluctuations (Baldocchi et al. 2001). The surface energy balance was closed according to Barr et al. (2006). An energy closure fraction was estimated as $F = (\lambda E + H)/(R_N - G)$ by linear regression, forced through the origin, with R_N and G as the independent variables and

TABLE 2. Datasets used in the evapotranspiration estimation and validation through PMBL.

Experiment–data source	Years	Spatial resolution	Temporal resolution	Biome type	Reference
SMEX-02	2002	Eddy covariance footprint	30 min	Agroecosystems	Prueger et al. (2005)
GCIP	1996–1998	Eddy covariance footprint	30 min	Agroecosystems	National Research Council (1998)
Tropics	Varying between 1999 and 2006	Eddy covariance footprint	Monthly	Rainforest	Fisher et al. (2009)
FLUXNET	Varying between 2002 and 2006	Eddy covariance footprint	Monthly	Diverse biome from forest, grassland, agroecosystem, wetland, and savanna	Baldocchi et al. (2001)

$H + \lambda E$ as dependent variables. This regression approach provided a stable and robust estimate of F across the entire range of $R_N - G$. We could also evaluate the PMBL λE across all the sites because an independent measurement of λE was available. Detailed descriptions of the different datasets (Table 2) are given below, and the distribution of sites is shown in Fig. 2.

a. Data from SMACEX SMEX-02

The Soil Moisture–Atmosphere Coupling Experiment (SMACEX) (Prueger et al. 2005; Kustas et al. 2005) was conducted in conjunction with SMEX-02 during June–July 2002 in and around the Walnut Creek watershed (WCW) near Ames, Iowa. The landscape was an agroecosystem with an intensive corn and soybean production region that consisted of a network of 12 eddy covariance meteorological and flux (METFLUX) towers (6 soybean and 6 corn) (Table 3). Multiple flight tracks were also flown by a Canadian Twin Otter aircraft for evaluating the spatial variability in surface fluxes across the study area. Surface fluxes (H, λE, and G), R_N, T_a, and RH were available at half-hourly intervals through the towers. At all the sites, tower heights were maintained at approximately $2h$ (where h is canopy height in meters) above the surface. All of the raw data were stored during the intensive observation period for consecutive 18 days from day of year (DOY) 171 to 189.

b. Data from the GCIP

The National Oceanic and Atmospheric Administration (NOAA)/Atmospheric Turbulence and Diffusion Division (ATDD) started operation of a long-term flux monitoring site near Bondville, Illinois, in 1996. This falls under the GCIP Enhanced Observing Period (EOP)

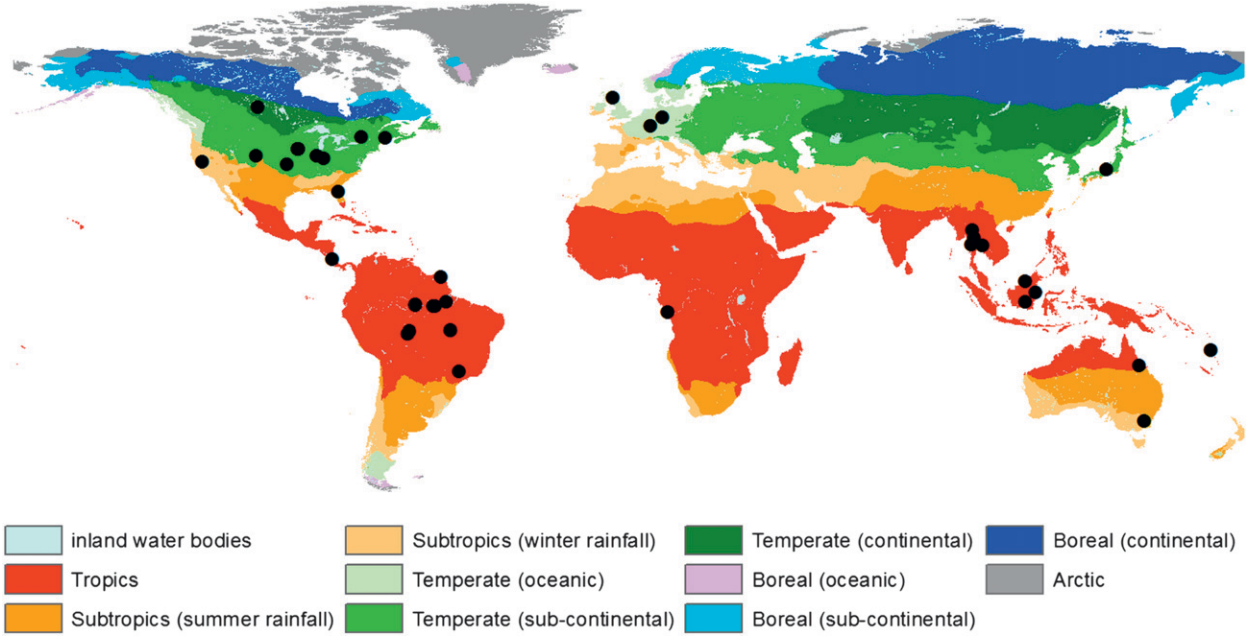

FIG. 2. Distribution of eddy covariance sites used in the present analysis over the prime climate zones of the world.

TABLE 3. Error statistics of the PMBL-derived λE over the eddy covariance sites of SMEX-02 and GCIP for both hourly and daily estimates.

					Hourly			Daily		
Experiment	Latitude (°)	Longitude (°)	Tower site ID	Crop	RMSE (W m^{-2})	MB (W m^{-2})	r	RMSE (W m^{-2})	MB (W m^{-2})	r
SMEX-02	41.983	−93.754	WC03	Soybean	37.0	−4.9	0.93	18.9	−7.2	0.75
	41.932	−93.753	WC06	Corn	43.6	−10.0	0.94	22.0	−19.7	0.89
	41.952	−93.687	WC13	Soybean	48.1	23.7	0.89	40.8	33.6	0.52
	41.945	−93.696	WC14	Soybean	53.0	−0.8	0.90	21.2	−2.5	0.75
	41.992	−93.535	WC23	Soybean	38.0	1.2	0.89	18.5	9.6	0.91
	41.992	−93.528	WC24	Corn	56.5	−21.4	0.90	13.0	1.8	0.88
	41.942	−93.539	WC25	Soybean	50.9	8.63	0.92	15.9	6.7	0.96
	41.975	−93.644	WC33	Corn	48.6	−3.7	0.90	24.6	21.8	0.97
	41.937	−93.663	WC151	Corn	41.5	−1.7	0.96	15.0	10.1	0.84
	41.937	−93.664	WC152	Corn	38.3	−5.9	0.95	10.6	−5.6	0.91
	41.934	−93.662	WC161	Soybean	35.6	−7.8	0.92	31.1	17.3	0.24
	41.935	−93.664	WC162	Soybean	40.3	−6.6	0.91	19.1	3.1	0.68
			Pooled	—	44.9	−2.0	0.90	20.9	5.8	0.78
			SMACEX aircraft	Corn–soybean mix	38.5	−0.4	0.90	—	—	—
			All corn		46.2	−5.1	0.92	—	—	—
			All soybean		44.6	10.9	0.90	—	—	—
GCIP	40.000	−88.280	Bondville	Corn	41.6	8.6	0.90	—	—	—
			Bondville	Soybean	34.6	−3.3	0.94	—	—	—
			Bondville	Corn	41.6	3.4	0.91	—	—	—

program that took place in the Mississippi River basin during 1995–2000. The field consisted alternately of soybeans and corn from 1996 to 1999. Half-hourly observations of surface fluxes (H, λE, and G) along with radiation and meteorological variables (e.g., R_N, T_a, and RH), were available at this site. The entire dataset and its detailed description are available through http://data.eol.ucar.edu/codiac. In the present study, we used data for three consecutive years from 1997 to 1999.

c. Data from the tropical forest

The study sites (21 sites) included a wide range of tropical biome types spreading around South America, Southeast Asia, Africa, and Oceania (Table 4). Micrometeorological instruments were attached to towers extending above the tall forest canopies. Energy balance closure at the tropical forest sites in this analysis was 80% for monthly daytime averages (Fisher et al. 2009). Monthly average of λE, H, R_N, G, T_a, and RH data was used based on averaging of half-hour to daily to monthly values.

d. Data from FLUXNET

These data cover a broad spectrum of biomes, climate, and plant functional types from 15 eddy covariance sites. The sites covered five subnetworks of FLUXNET (Baldocchi et al. 2001): AmeriFlux, AsiaFlux, EuroFlux, Fluxnet Canada, and OzFlux. Here also independent measurement of λE was available, along with measurements of H, R_N, G, T_a, and RH. A comprehensive description of this dataset can be found in Fisher et al. (2008).

e. PT-JPL model

The specific reason of selecting the tropics and FLUXNET sites was to compare the PMBL results with another model [Priestley–Taylor–Jet Propulsion Laboratory (PT-JPL)] (Fisher et al. 2008, 2009) output that was based on constraining the Priestley–Taylor parameter (α) over a wide range of hydroclimatic regimes. PT-JPL is a global model for estimating λE that is based on the Priestley and Taylor (1972) PE framework, where different biophysical and meteorological scalars were used to constrain PE into λE. PT-JPL runs with five inputs: R_N, two vegetation indices, T_a, and e_a, to generate spatially explicit and temporally consistent λE estimates. Given that the results from Fisher et al. (2008, 2009) were monthly, PMBL was also executed on the monthly scale over the tropics and FLUXNET.

5. Results

a. Validation of latent heat flux

1) SMEX-02–SMACEX AND GCIP

PMBL was run at a temporal resolution of 30 min over the 19 days of the intensive observation period at each of the 12 flux tower sites of SMEX-02. The overall

TABLE 4. Intercomparison of PMBL λE statistics against λE observations and PT-JPL λE model for individual eddy covariance sites of the tropical forest eddy covariance subnetwork.

				λE_{PMBL}			$\lambda E_{\text{PT-JPL}}$		
Tropics EC subnetwork	Site	Latitude (°)	Longitude (°)	RMSE (W m^{-2})	MB (W m^{-2})	r	RMSE (W m^{-2})	MB (W m^{-2})	r
Africa	Kissoko (KIS)	−4.791	11.982	19.0	14.7	0.96	35.6	32.4	0.96
South America	Bannanal Island (BAN)	−9.824	−50.159	28.6	−11.5	0.78	23.2	17.9	0.89
	Caxiuana (CAX)	−1.719	−51.458	18.8	8.2	0.97	36.1	33.9	0.98
	Fazenda Noza Senhora (FNS)	−10.761	−62.357	16.1	15.0	0.97	28.1	27.5	0.97
	Guyaflux (GUY)	5.277	−52.928	17.3	−5.5	0.62	19.5	13.2	0.76
	La Selva (LAS)	10.423	−83.978	52.1	−45.5	0.96	31.1	−22.5	0.97
	Manaus C14 (M14)	−2.589	−60.115	8.8	3.0	0.97	12.8	9.9	0.97
	Manaus KM34 (M34)	−2.609	−60.209	5.1	−1.7	0.97	11.1	10.1	0.97
	Reserva Jaru (RJA)	−10.083	−61.931	9.4	−6.0	0.90	13.3	11.2	0.91
	Reserva Pé-de-Gigante (RPG)	−21.619	−47.649	23.8	0.3	0.91	29.7	21.2	0.92
	Santarem KM67 (KM67)	−2.856	−54.958	8.0	−4.9	0.95	17.0	15.3	0.93
	Santarem KM77 (KM77)	−3.011	−54.536	45.9	27.5	0.68	63.0	55.4	0.80
	Santarem KM83 (KM83)	−3.018	−54.971	18.9	−17.7	0.95	6.7	0.7	0.95
Oceania	Cocoflux (COC)	−15.435	167.185	12.4	−4.8	0.88	17.9	12.3	0.88
Southeast Asia	Bukit Soeharto (BKS)	0.868	117.052	22.6	14.9	0.79	29.7	22.5	0.79
	Kog-Ma (KOG)	18.800	98.900	20.1	−3.6	0.31	15.6	5.2	0.64
	Lamber Hills (LAM)	4.200	114.033	10.2	6.8	0.98	24.4	12.1	0.98
	Mae Klong (MKL)	14.582	98.850	6.6	−4.5	0.81	5.9	1.6	0.73
	Palangkaraya (PKA)	−1.655	114.036	14.9	−11.4	0.92	13.8	10.2	0.92
	Sakaerat (SKR)	14.485	101.926	25.1	5.7	0.86	32.0	21.2	0.87
	Tak (TAK)	16.622	99.433	13.6	3.2	0.78	12.5	6.8	0.87
Pooled	—	—	—	23.8	−0.4	0.92	28.4	17.1	0.93
Annual (mm)	—	—	—	103	2	0.95	111	157	0.94

root-mean-square error (RMSE) and mean bias (MB) of the predicted half-hourly λE from the 12 towers were −1.97 and 44.9 W m^{-2} with a correlation (r) of 0.90 (Table 3), respectively. The RMSE of individual sites varied between 35.6 and 57.5 W m^{-2} with an r of 0.88–0.96 (Table 3). On the daily scale, the RMSE varied from 13 to 31.1 W m^{-2}, with an overall RMSE of 20.9 W m^{-2} (Table 3). To determine the ability of the PMBL approach to accurately track the land surface fluxes, a time series comparison between modeled λE and those from eddy covariance measurements was performed. Two representative sites (one corn and one soybean; Figs. 3a,c) were selected to show the diurnal dynamics of λE and characterize the response of two different crop types on modeled λE during the daytime hours from DOY 171 to 189. Figures 3a,c reveal that the temporal λE dynamics from PMBL over both the corn and soybean were consistent with the observed λE pattern thorough out the study period. Observed λE over the corn was about 80–120 W m^{-2} greater than the soybeans, and PMBL could clearly detect this difference. Scatterplots of λE predictions from PMBL against measured λE at all the corn and soybean tower sites revealed the performance of PMBL to be relatively better over the soybean, as compared to the corn (Figs. 3b,d; Table 3). This, we think, could be because of the relatively uniform vegetation cover of soybean canopy as compared to the larger variability seen for corn canopies. For the soybean sites, an even distribution of points around the 1:1 validation line (Fig. 3d) indicates a good fit of predictions with the measured λE, with r and RMSE of 0.90 and 44.6 W m^{-2} and having slope and offsets of r to the order of 0.96 (±0.01) and 19 (±3.7), respectively. For the corn sites, r and RMSE of 0.92 and 46.2 W m^{-2} (Fig. 3b; Table 3) was obtained with a slope and offset of r to the order of 0.86 (±0.01) and 32.3 (±3.1).

Transect-averaged λE from DOY 166 to 186, observed by the Canadian Twin Otter at 40 m above ground level for the 16 aircraft flights, revealed an RMSE and r of 38.5 W m^{-2} (14% of the observed mean) and 0.90 (Table 3; Figs. 3e,f). The data of individual flight tracks are pooled together, and the temporal comparison of the PMBL λE with the aircraft fluxes revealed a coherent behavior (Fig. 3e).

The validation results over GCIP were equally promising, with a correlation between the predicted and measured λE to be 0.90, 0.94, and 0.91 for the three individual crop years (1997, 1998, and 1999). The RMSE for all the three years was 41.6, 34.6, and 41.6 W m^{-2}

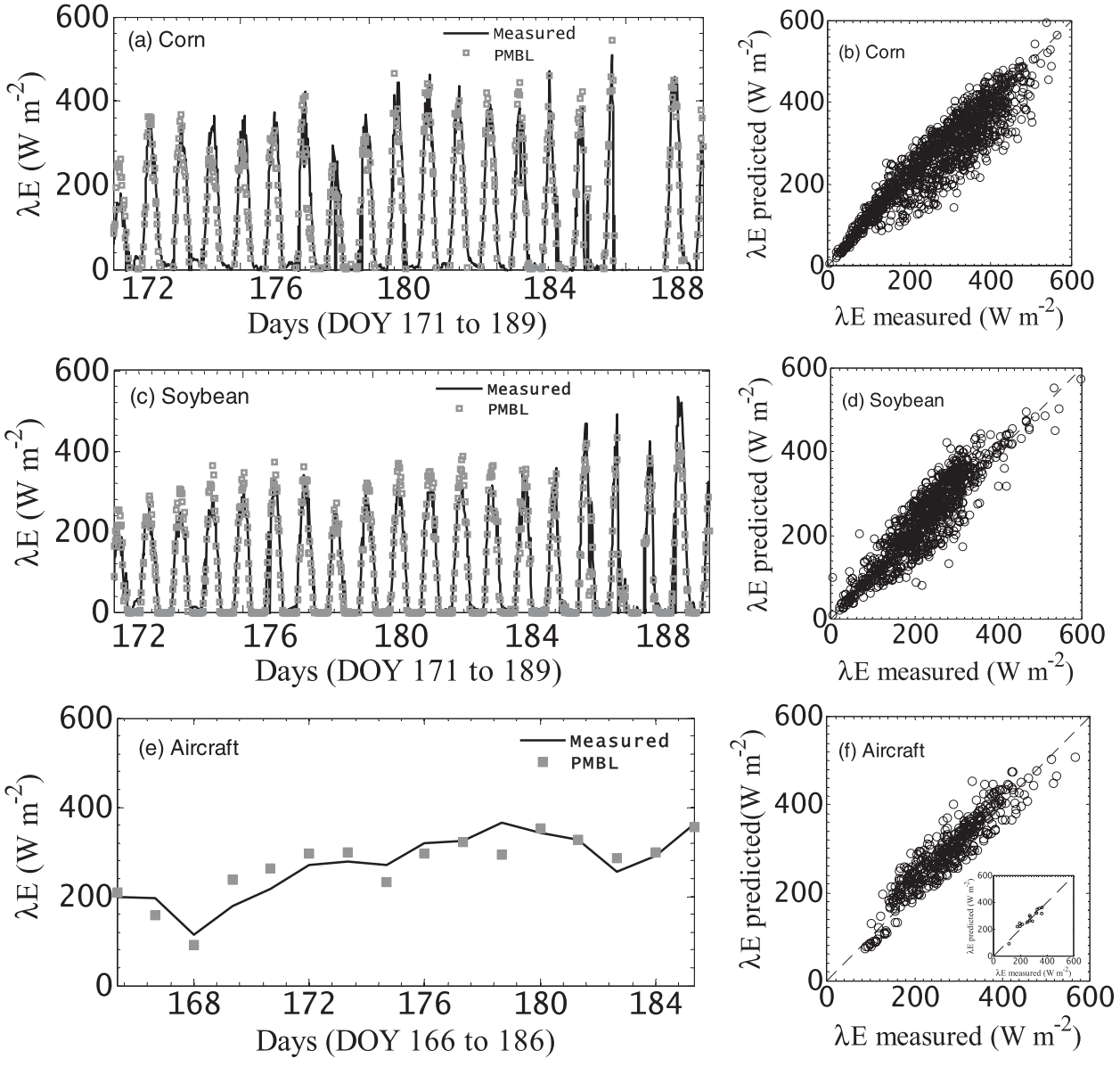

FIG. 3. Time series comparison of observed λE (black line) and PMBL predictions (gray squares) for (a) corn (WC33), (c) soybean (WC03), and (e) aircraft-measured during SMEX-02, along with the pooled validation of λE for all the (b) corn, (d) soybeans, and (f) aircraft transect flight paths for every individual day during SMEX-02. In (e), the transect data along flight paths of every individual day were averaged to produce the time series. The plot in the inset of (f) is the 1:1 validation of transect-averaged λE vs PMBL λE. Any gap in the time series is caused either by the absence of flux measurements or missing ancillary data.

(Table 3). An illustrative example of the 1:1 validation plot (Fig. 4a) for the year 1998 revealed a good fit of the λE predictions, with a slope and offset of 0.95 ($\pm$0.004) and 1.93 ($\pm$0.52). The temporal comparison (Fig. 4b) of the measured and predicted λE during the active vegetative phase of soybeans revealed the efficacy of the proposed approach in tracking the pattern of λE for both the high and low magnitude.

Having retrieved λE, we also assessed the magnitude of surface energy balance closure $[(\lambda E + H)/(R_N - G)]$ based on the estimated λE and observed H, R_N, and G. The magnitude of closure was 75% for SMEX-02 and 78% for the GCIP.

2) TROPICAL EDDY COVARIANCE AND FLUXNET

The approach was also applied on monthly data over 21 different tropical rain forest locales. The evergreen rain forest sites spanning over the equatorial band showed the best results (Table 4) with an overall RMSE

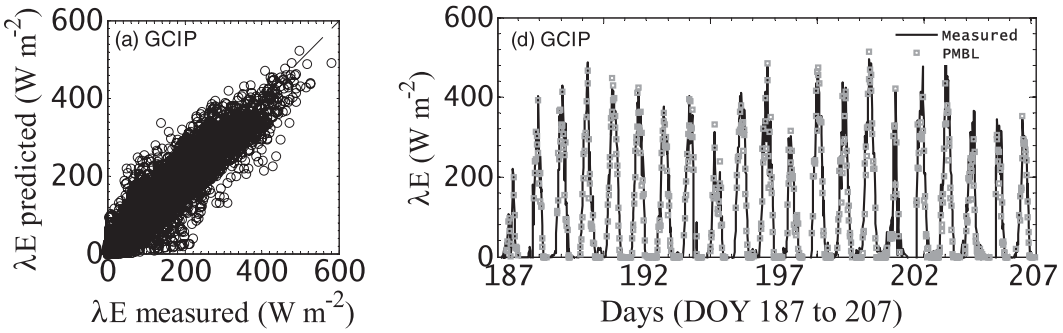

FIG. 4. (a) Pooled 1:1 validation of measured vs PMBL λE over the eddy covariance sites of Bondville during GCIP for the year 1998. This produced a correlation of 0.94 with a gain and offset of correlation 0.95 ($\pm$0.004) and 1.93 ($\pm$0.52), respectively. (b) Comparison of time series of tower measurements (black line) vs PMBL (gray squares) λE during the active vegetative phase of soybeans in 1998.

of 23.8 W m^{-2} and an r of 0.92 (Table 4). The RMSE varied between 6.6 and 52.1 W m^{-2} across the tropical rain forest sites, with r varying from 0.31 to 0.98 (Table 4). Among all the sites, maximum RMSE (52.1 W m^{-2}) was obtained for the La Selva (LAS) site. All the Amazon sites (BAN, CAX, M14, M34, KM67, and KM83) in the South America subnetwork showed consistently good results, with the exception of the KM77 site, where RMSE was relatively high (45.9 W m^{-2}; see Table 4 for the complete list of sites and their abbreviations). An intercomparison of our λE with the PT-JPL λE (Table 4) revealed nearly similar statistics, and the difference in the overall RMSE between the two approaches was only 4.6 W m^{-2}. Sitewise comparison revealed the maximum difference in RMSE between the two approaches to be approximately 20 W m^{-2}.

The λE estimates from our method over the 15 FLUXNET sites also produced good agreement with the observations and captured nearly 90% variability of the monthly λE, with an RMSE of 29 W m^{-2} or approximately 15 mm month^{-1} (Table 5). RMSE varied between 8.5 and 53.7 W m^{-2}. Overall, r between the predicted and measured λE was 0.89. Here also, an intercomparison of our λE with the PT-JPL λE estimates was done and is summarized in Table 5. The maximum difference in RMSE between the two approaches was found in Virginia Park (around 18 W m^{-2}). For rest of the FLUXNET sites, the RMSE difference between the two approaches varied from 5 to 10 W m^{-2}. However, the mean bias revealed a consistent overestimation of λE by both PMBL and PT-JPL over a majority of the sites (Table 5).

Illustrative examples of the temporal dynamics of tropical forest λE over two continents (South America and Southeast Asia) falling under diverse climatic settings are shown in Figs. 5a,b. The example revealed the efficacy of the proposed approach in capturing both the high-frequency and low-frequency fluctuations in the monthly λE. Similarly, the temporal pattern of λE over a broad range of biomes in the FLUXNET eddy covariance network (Figs. 5c,h) also revealed the efficiency of the proposed approach to track the year-round dynamics in λE.

Given the significance of λE as an essential climate variable, annual evaporation (E) was also analyzed for both the tropics and FLUXNET sites (Figs. 6a–d). Annual evaporation was computed by summing the monthly values. If, in any year, an observed or estimated E value in a month was missing, that particular year was not included in the computation. Over the tropics, the overall RMSE of annual E from our approach was 103 mm (Table 4), which was 13% of the observed mean, as opposed to 157 mm from the PT-JPL. For the FLUXNET sites, an overall RMSE of 119 mm (Table 5) was obtained with PMBL, which was higher than the RMSE obtained by PT-JPL (110 mm yr^{-1}). The overall correlation between the proposed approach and observed annual E was 0.95 over the tropics and 0.86 over the FLUXNET, respectively. An overestimation tendency of annual E over the FLUXNET sites for both PMBL and PT-JPL was evident from Table 5 and Figs. 6c,d.

The South American subnetwork of towers was mostly concentrated in Amazonia. Observed annual E varied between 548 and 1243 mm across all the Amazon basin stations, and our estimates varied between 536 and 1208 mm (Fig. 6b). In South America, the highest E was found in LAS at about 1243 mm with a very high interannual and month-to-month variability. Over Southeast Asia, the variability of the annual E is quite high among sites, with a range varying from as low as 240 mm [Mae Klong (MKL)] to as high as 1209 mm [Palangkaraya (PKA)] (Fig. 6b). The E outputs from PMBL have also captured a similar pattern,

TABLE 5. Intercomparison of PMBL λE statistics against λE observations and PT-JPL λE model for the individual eddy covariance subnetwork of FLUXNET. Abbreviations: CRO, cropland; GRA, grassland; DBF, deciduous broadleaf forest; ENF, evergreen needleleaf forest; EBF, evergreen broadleaf forest; WET, wetland; and SAV, savanna.

					λE_{PMBL}			$\lambda E_{\text{PT-JPL}}$		
FLUXNET	Site	Biome	Latitude (°)	Longitude (°)	RMSE (W m^{-2})	MB (W m^{-2})	r	RMSE (W m^{-2})	MB (W m^{-2})	r
AmeriFlux	Bondville (BOND)	CRO	40.006	−88.290	21.6	5.6	0.97	23.6	5.4	0.96
	Howland (HOW)	ENF	45.204	−68.740	38.8	29.0	0.89	26.3	−4.9	0.94
	Mize (MIZ)	ENF	29.764	−82.245	33.0	2.7	0.83	25.5	2.7	0.93
	Morgan Monroe (MMS)	DBF	39.323	−86.413	34.9	22.9	0.97	32.3	29.0	0.98
	Niwot Ridge (NR)	ENF	40.033	−105.546	26.7	20.5	0.93	15.3	−3.0	0.95
	Tonzi Ranch (TON)	SAV	38.432	−120.966	30.4	11.1	0.79	25.4	14.3	0.87
	Walnut River (WAL)	GRA	37.521	−96.855	25.8	3.6	0.94	9.4	−3.7	0.99
EuroFlux	Griffin (GRIF)	ENF	56.607	−3.798	11.7	−5.8	0.97	12.7	−2.7	0.96
	Hainich (HAI)	DBF	51.079	10.452	17.9	12.6	0.95	23.4	17.0	0.96
	Hesse (HES)	DBF	48.674	7.064	18.7	11.8	0.97	22.8	18.0	0.98
Fluxnet Canada	Mer Bleue (MER)	WET	45.409	−75.519	8.5	1.3	0.99	17.2	2.3	0.98
	Northern Study Area–Old Black Spruce (OBS)	ENF	53.987	−105.118	19.9	15.0	0.91	11.5	−2.1	0.91
OzFlux	Tumbarumba (TUM)	EBF	−35.656	148.152	33.7	25.0	0.92	23.5	0.7	0.91
	Virginia Park (VIR)	SAV	−19.883	146.553	53.7	47.6	0.60	37.0	34.3	0.89
AsiaFlux	Takayama (TAK)	DBF	36.146	137.423	21.9	17.7	0.92	33.4	29.0	0.88
Pooled	—	—	—	—	29	13.1	0.89	23.6	9.5	0.95
Annual (mm)	—	—	—	—	119	83	0.86	101	53	0.86

thus revealing its potential to capture the wide variability of annual E in Southeast Asia. Among the five subnetworks of FLUXNET, the maximum among site variability in annual E (371–823 mm) was found in AmeriFlux and the minimum variability (341–448 mm) was found within the EuroFlux. This pattern was also captured by our approach (Fig. 6d); however, its performance was relatively weaker for the five sites (HOW, NR, MMS, TUM, and VIR; see Table 5 for full site names) where annual E was significantly overestimated (Fig. 6d).

Observational evidence of the decline in the annual E over the central Amazon was noted for the year 2005, and our approach also captures this well. For example, there was a sharp decrease of 33% in the annual E from 630 to 420 mm in the Manaus KM34 (M34) between 2000 and 2006 (Fig. 7a). The annual E over Ecotonal Bannanal plantation reduced about 17% from 2004 to 2005 (Fig. 7b). M34 has often been treated as a benchmark reference site for land atmosphere interaction studies over the Amazon (Pielke et al. 2011), and this sharp decline in the annual E supports the extended drought period in the Amazon that was initiated by an El Niño in 2002/2003, followed by warming of the tropical Atlantic sea surface in 2004/2005. The decline in rainfall for the 2004/2005 drought was moderate, but because it followed on the heels of an El Niño, the rainforest had a limited wet spell in between the two dry periods and could not recharge.

b. *Analysis of canopy conductance (g_S)*

1) g_S VERSUS VPD AND λE

(i) SMEX-02–SMACEX and GCIP

Since no observation of g_S was available, its validation could not be possible. Analysis of g_S was carried out in relation to the observed global radiation (R_G) [or photosynthetically active radiation (PAR)], VPD, and λE (Niyogi and Raman 1997). The magnitude of g_S during SMEX-02 varied between 0.001 and 0.05 m s^{-1} for both of the crops, and no significant difference in g_S was obtained between the two crops, with a mean g_S of around 0.015 m s^{-1}. Clearly, g_S was 0 m s^{-1} at night in the absence of net available energy. A plot of g_S with VPD (Figs. 8a,b) revealed that g_S reached a maximum level under low VPD and decreased with increasing VPD. For both corn and soybeans, g_S showed a sharp exponential decrease (negatively logarithmic) with an increase in the VPD pattern, depending upon varying degrees of R_G. Figure 8a shows the responses of g_S to VPD separated by five different levels of R_G groups. Five negatively logarithmic scatters fit the data with r values of 0.62 ($0 < R_G < 150$ W m^{-2}), 0.84 ($150 < R_G < 300$ W m^{-2}), 0.88 ($300 < R_G < 450$ W m^{-2}), 0.86 ($450 < R_G < 600$ W m^{-2}), and 0.85 ($R_G > 600$ W m^{-2}). For soybeans, the r values of the exponential scatter (Fig. 8b) for the similar five levels of R_G were 0.64, 0.85, 0.89, 0.85, and 0.82. For both the crops, the sensitivity of g_S to VPD was at a maximum in the R_G range of 300–450 W m^{-2} and the sensitivity of

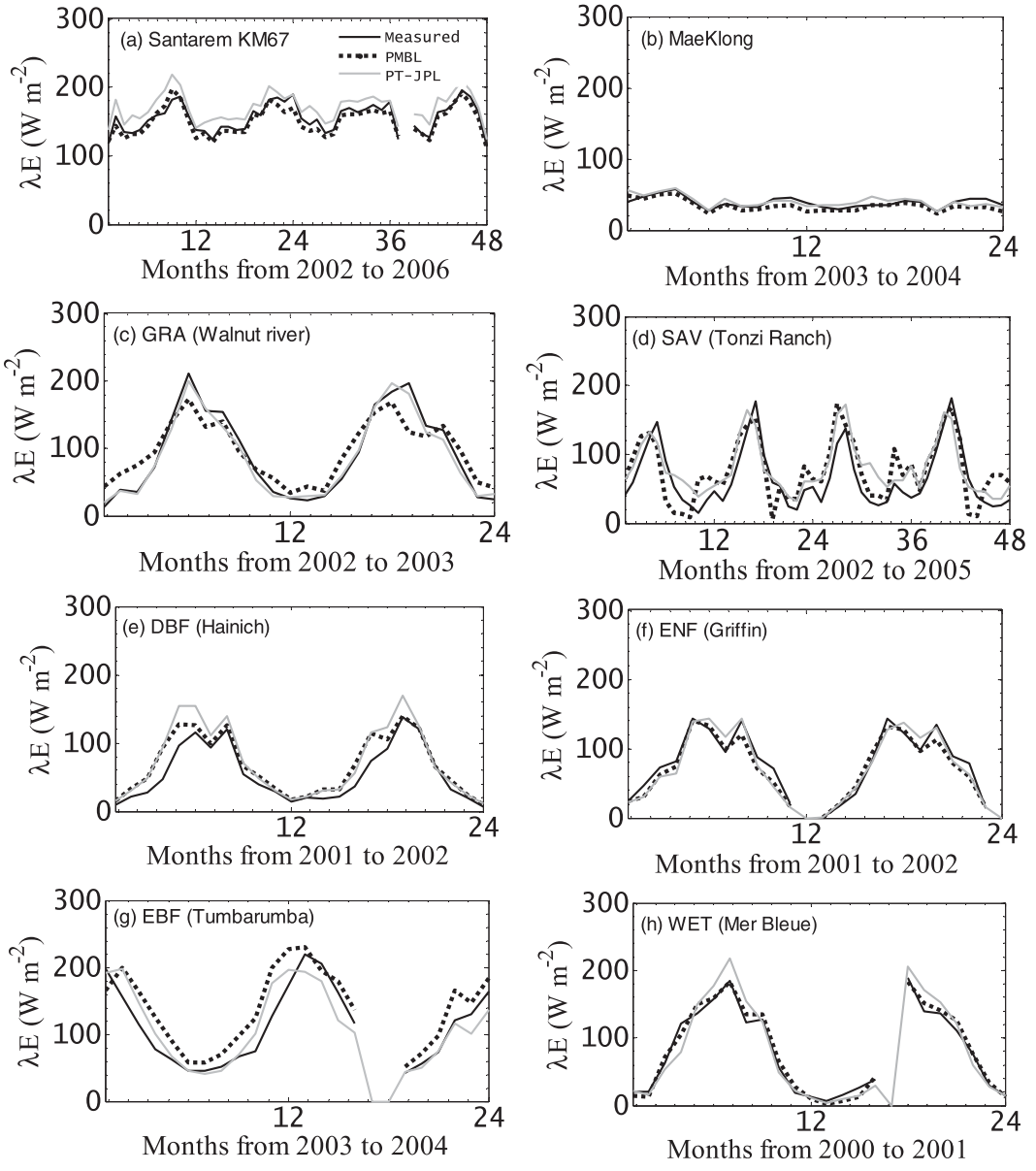

FIG. 5. (b) Comparison of time series of tower measurements vs PMBL and PT-JPL λE for the representative sites of the (a) South American (Santarem KM67), and (b) Southeast Asian (Mae Klong) subnetworks; (c)–(h) similar comparison over representative sites covering six broad spectrums of biome types of the FLUXNET eddy covariance network.

g_S to VPD decreased when R_G was lesser than 150 W m^{-2} (Niyogi et al. 1998).

Two dimensional scatters between g_S and observed λE (Figs. 8c,d) revealed linearity when plotted for different levels of VPD. This shows that g_S tends to decrease with increasing VPD without any increase in the λE, like an inverse hyperbolic pattern to VPD (Monteith 1995). Stomatal regulation tended to keep the λE constant when the VPD was changed from low (10–15 hPa) to high magnitude (>25 hPa) (Figs. 8c,d). This also revealed the sensitivity of g_S to λE to be directly proportional to VPD. The correlation of the scatter between g_S and λE for the varying levels of VPD was highest ($r = 0.91$ for corn and $r = 0.89$ for soybeans) at $20 > \text{VPD} > 10$ hPa. The least correlation (0.40 for corn and 0.35 for soybeans) was found at VPD < 5 (Figs. 8c,d).

Illustrative examples of the diurnal pattern of g_S for both corn and soybeans (Figs. 8e,f) revealed that g_S closely follows the shortwave radiation (R_G) pattern, and peak g_S was found before the noon (between 1000

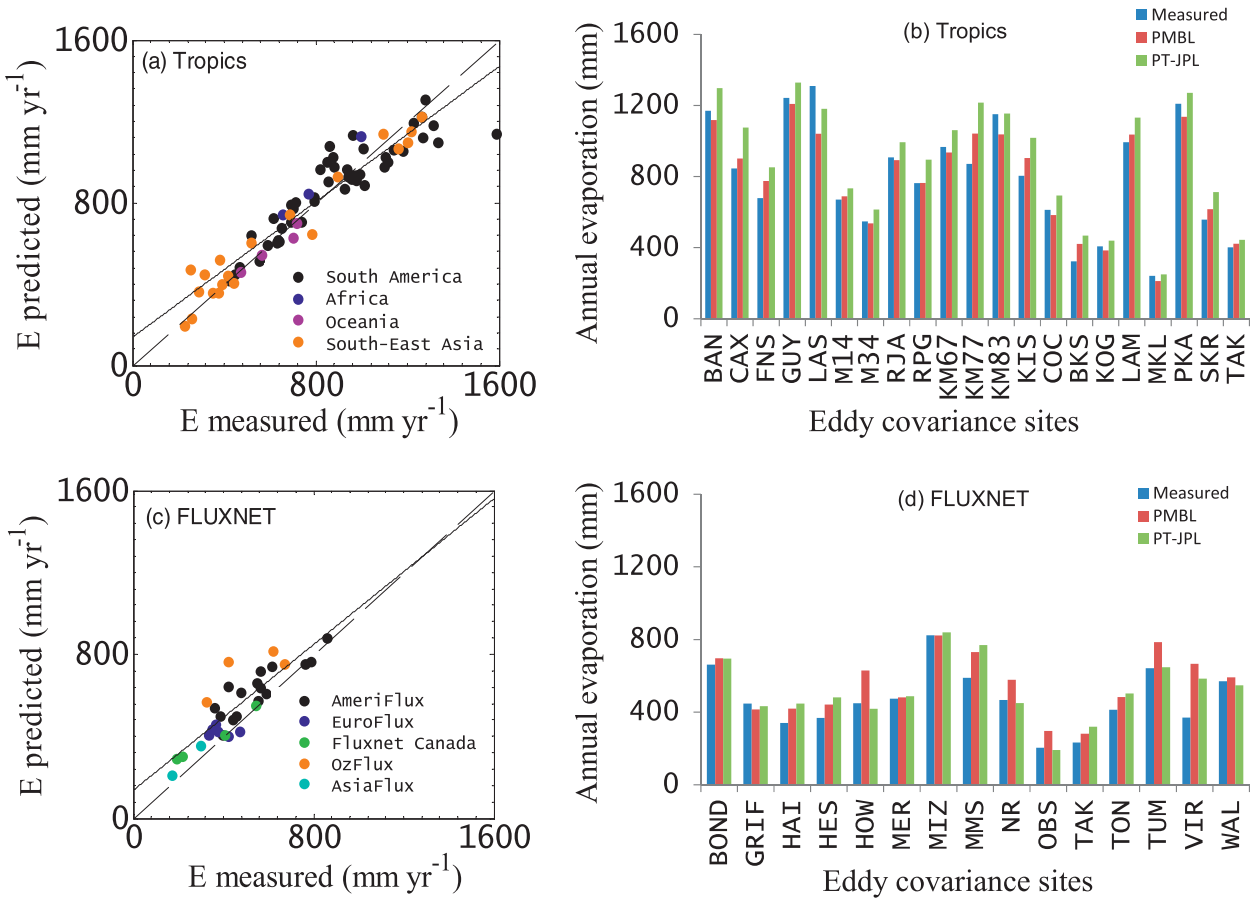

FIG. 6. (a) Validation of individual year-wise annual E over the tropics using PMBL. PMBL produced an overall r of 0.95 (R^2 = 0.90), with a slope and offset of r (black solid line) to be 0.83 (±0.03) and 136.15 (±28.69), respectively. (b) Histogram comparison of mean annual E between PMBL and PT-JPL by averaging all the individual year E values over 21 tropical eddy covariance sites. The number of years in this averaging varied from at least three to a maximum of seven. (c),(d) As in (a),(b), but over only the FLUXNET sites; PMBL produced an overall r of 0.87, with a slope and offset of r (black solid line) to be 0.89 (±0.09) and 135.05 (±45.58), respectively. The histograms are from 15 FLUXNET sites. The number of years in this averaging varied from at least two to a maximum of five.

and 1100 LT) when the water use efficiency was high because of ample R_G and low saturation deficits. Thereafter, g_S decreased steadily for the rest of the day as VPD increased, and R_G levels fell in the afternoon. Because of multiple controls on g_S, particularly the strong control of R_G at midday, the diurnal patterns of g_S did not show a negative correlation with VPD until it followed a certain level of R_G during the course of a day (Figs. 8e,f). Once it attained its peak, g_S started falling in the afternoon, even with the increase in R_G and VPD (Niyogi et al. 2009).

For the GCIP also, g_S was strongly reduced with an increase in VPD; about a 50% reduction was noted when VPD increased from 10 to 20 hPa. The negative logarithmic relationship between g_S and VPD was found by grouping g_S on the basis of R_G on the half-hour temporal data. Five negatively logarithmic scatters (Fig. 9a) fit the data with r values of 0.58 ($0 < R_G <$ 150 W m^{-2}), 0.61 (150 $< R_G <$ 300 W m^{-2}), 0.66 (300 $<$ $R_G <$ 450 W m^{-2}), 0.66 (450 $< R_G <$ 600 W m^{-2}), and 0.69 ($R_G >$ 600 W m^{-2}). The correlation coefficients of the exponential scatters are again indicative of the high sensitivity of g_S to VPD for the magnitude of R_G at or above 150 W m^{-2}. Here also, the correlation of the scatter between g_S and λE for the varying levels of VPD was highest (r = 0.81) at 10 $<$ VPD $<$ 15 hPa, and the relationship strength was lowest at VPD $<$ 5 hPa (Fig. 9b).

Diurnal behavior of g_S with R_G and VPD during GCIP was very similar to that observed over SMEX-02. An example of diurnal dynamics for five consecutive days during the active growth stage of soybeans clearly revealed a midday depression in g_S, which may be caused by peak VPD at midday (Fig. 9c). For relatively good moisture availability, g_S responds directly to rising R_G in the morning hours; in the later part of the day, it inversely

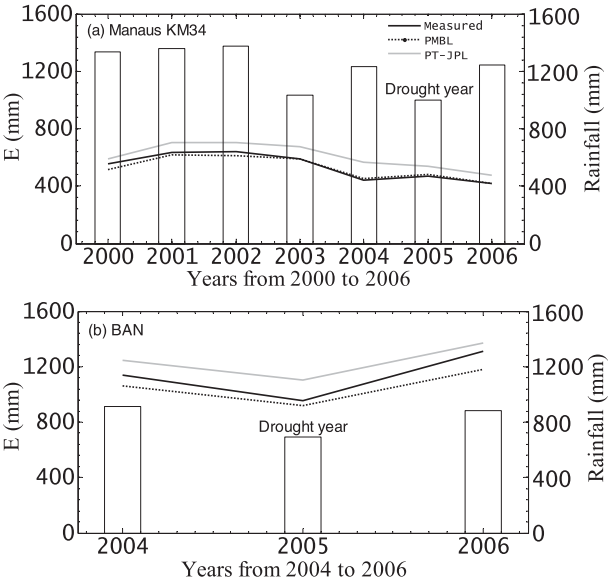

FIG. 7. Time series of annual E over two representative sites: (a) Manaus KM34 (central Amazon) and (b) Bannanal Island (BAN) (southern Amazon) of the Amazonian rain forest. This clearly shows a significant decrease in the E during 2004/2005, and PMBL is capable of capturing this declining trend in E for 2004–05 along with PT-JPL.

responds to increasing VPD, and again, in the very late afternoon, it responds directly with decreasing R_G. Thus, the maximum value of g_S is mostly found in the morning (Niyogi et al. 2009).

(ii) Tropical forest and FLUXNET

The magnitude of monthly g_S over the tropics varied from 0.005 to 0.035 m s^{-1}. As in previous experiments, here also the scatters between g_S and VPD revealed an exponential decline of g_S with rising VPD (Fig. 10a). Three exponential scatters fit the data with r values of 0.51 ($0 < R_N < 150$ W m^{-2}), 0.54 ($150 < R_N < 300$ W m^{-2}), and 0.66 ($300 < R_N < 450$ W m^{-2}). Linear response of g_S with λE (Fig. 10b) for different thresholds of VPD was also found. A 50% reduction in the g_S was found with a rise in VPD from 10 to 20 hPa at a constant level of λE.

The nature of scatter and correlation between g_S versus VPD and g_S versus λE was similar over the FLUXNET (Figs. 10c,d). The correlation of the exponential scatter between g_S and VPD was maximum (0.66) for $300 < R_N < 450$ W m^{-2} and least (0.51) for $R_N < 150$ W m^{-2}. Similarly, the correlation of the linear scatter between g_S and λE was maximum (0.98) for VPD > 25 hPa and least (0.64) for VPD < 5 hPa.

2) g_S VERSUS GROSS PRIMARY PRODUCTION

Given g_S is the "coupler" between λE and photosynthesis [net primary productivity (NPP)], the dependence of g_S on gross primary production (GPP) is also analyzed (NPP data were not available). Figures 11a,b show the response of GPP to g_S. After an initial increase, the response of GPP became asymptotic and the carbon gain slightly declined after a g_S of 0.02 m s^{-1}. Plants use their stored carbon conservatively; they are much more efficient in controlling g_S when atmospheric VPD is low and surface moisture is high in the morning hours, so that the stored carbon can be utilized later to moderate the impacts of high afternoon VPD (Niyogi and Xue 2006). Substantial diurnal hysteresis was found in the plot of g_S against GPP, VPD, and R_G (Fig. 11c). R_G represents the driving force for GPP, but VPD controls the g_S through imposing limitation on stomatal opening. Although R_G and VPD tend to covary throughout a day, their variation is out of phase on clear days. As a result, the variation of g_S is also out of phase with GPP.

c. Sensitivity analysis

Relative sensitivity of the derived λE to perturbations in four critical radiation and meteorological variables (Table 6) revealed λE to be the most sensitive to the uncertainties in the R_N, and an error in R_N of ±10% can produce a relative error of 22%–24% in the λE estimates (Niyogi et al. 1999). Among other variables, the relative humidity proved to be the second-most sensitive variable at a lower range (60%–70%), where a 10% uncertainty may produce an error of 12%. The sensitivity of λE to T_a and G was very small, 4%–8% and 4%–6%, respectively. Given the measurement accuracy of the current generation R_N (±10%), T_a (±2%), and RH (±1%) measurement sensors, the potential uncertainty of our estimates of λE may be 20%–25% if the sensor uncertainty is additive. However, the errors tend to cancel each other out if the uncertainties of the input variables are in the opposite direction. Uncertainty may be reduced when applied from the remote sensing platform because the accuracies of R_N, T_a, and RH from current generation satellites are 5 W m^{-2} (http://ceres.larc.nasa.gov/science_information.php), ±1K, and ±10% (Tobin et al. 2006), respectively. The current uncertainty analysis does not explicitly address sensitivity of PMBL to multiple variables. Multivariate sensitivity may either enhance the cumulative error or may cancel out each other's effects and thus may reduce the overall errors.

6. Discussion

For the experimental and tower network data, the residual error (predicted − observed) in the λE was influenced by M (RH^{VPD}) and VPD (Figs. 12a,d); T_a and Φ do not have much influence on the residual error

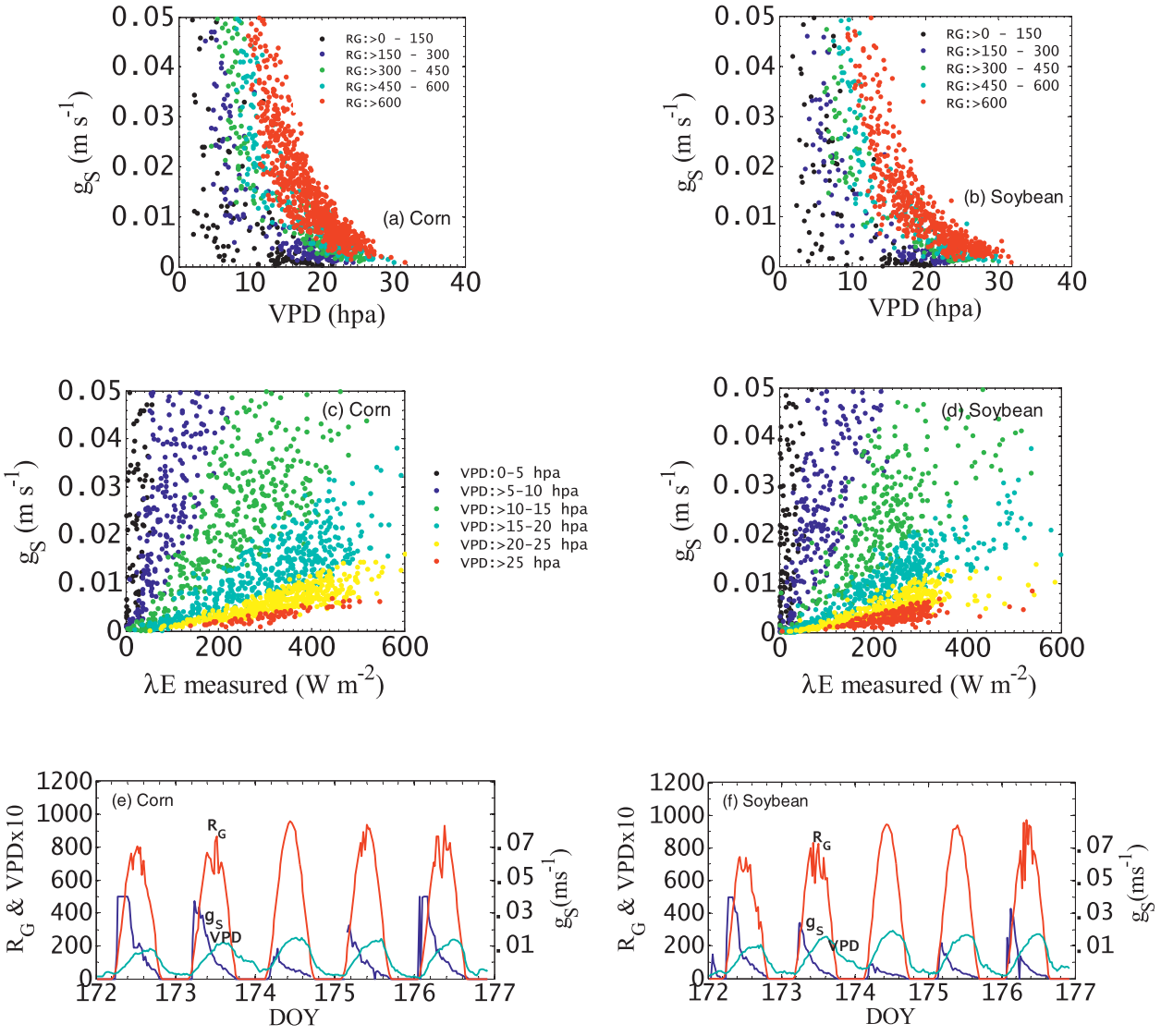

FIG. 8. Response of g_S to changes in the VPD for (a) corn and (b) soybeans during SMEX-02. The behavior of retrieved g_S with observed λE for different classes of VPD in (c) corn and (d) soybeans. (e) Illustrative examples of the diurnal patterns of g_S (blue line), R_G (W m^{-2}) (red line), and VPD (hPa) (green line) over five consecutive days for corn and (f) soybeans, respectively, during SMEX-02.

(Figs. 12b,c). This was evident for all of the sites where the residual error was negative (predicted < observed) up to M values of 0.25, and it was consistently positive beyond M values of 0.25 (Fig. 12a) up to $M = 0.75$. For the intermediate ranges of VPD (10–20 hPa), the residual error was consistently positive, whereas for VPD >20 hPa, the error was in both direction. The formulation of M is based on the hypothesis that equilibrium exists between atmospheric and surface moisture and under the condition of extreme surface dryness and high evaporative demand (VPD); no water vapor can be transferred into the atmosphere because of unavailability of water in the surface. The vapor pressure deficit was treated as a proxy to bridge between surface dryness and high evaporative demand, but such equilibrium assumption may be violated and VPD may not truly capture the entire dryness or wetness regime from the surface to subsurface. Plants can extract some moisture through roots to transpire if some moisture is present in the root zone. Under such conditions the RH^{VPD} expression may underestimate the wetness, and resultant λE will also be underestimated. This might be the reason for consistent underestimation of λE and higher RMSE in corn compared to soybeans, as reported in section 5a(1) and Table 3. Also, corn has spatially variable leaf area index (LAI) as compared to soybean. As a result the values of λE on corn have higher variability and also result in possible poor predictions as

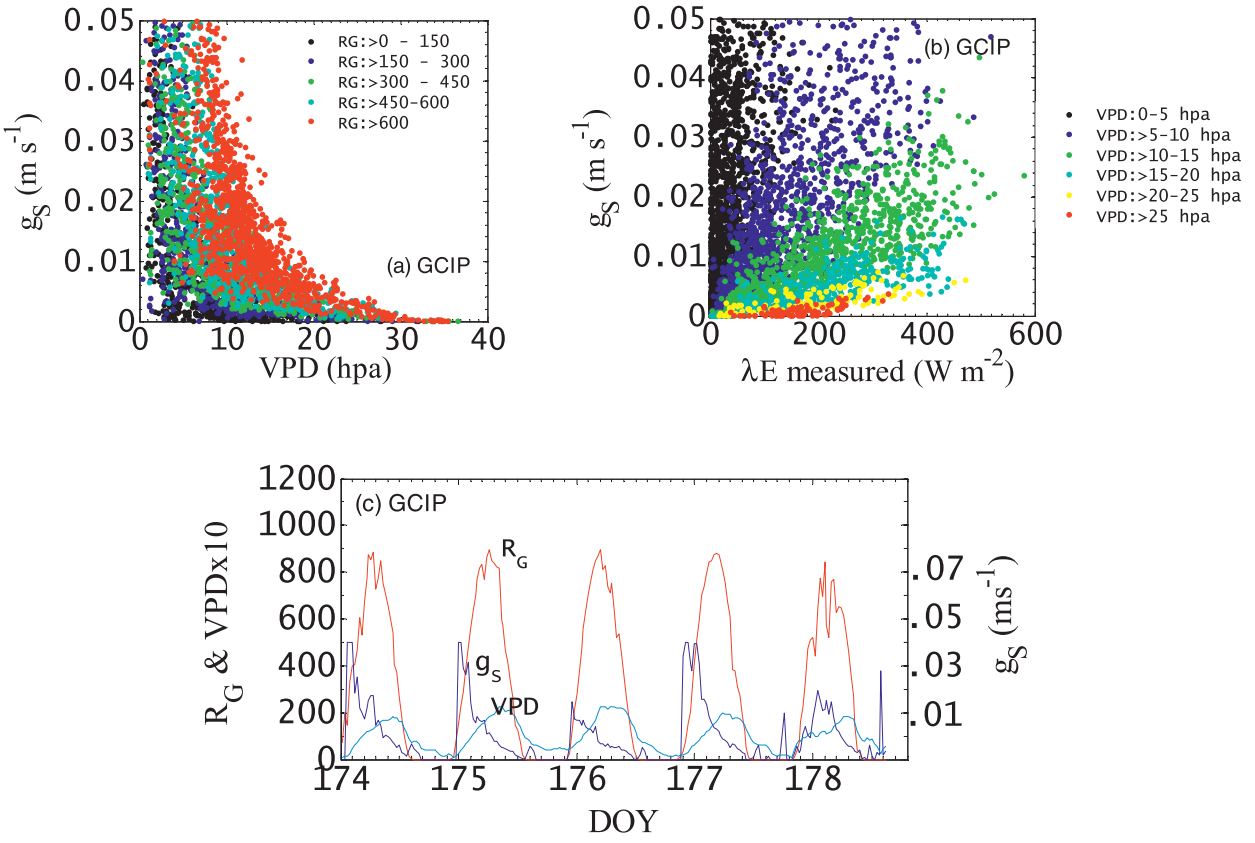

FIG. 9. (a) Response of stomatal conductance (g_S) in relation to VPD for different levels of R_G over the eddy covariance sites of Bondville during GCIP. (b) Dependence of λE on g_S for different levels of evaporative demand (VPD) over Bondville during GCIP. This example is shown pooling all the 30 min data for the year 1998. (c) Diurnal patterns of g_S (blue line), R_G (W m^{-2}) (red line), and VPD (hPa) (green line) over five consecutive days over Bondville during GCIP.

compared to the soybeans. Corn has a longer root length that is capable of extracting water from deeper layers. PMBL does not include any crop ecophysiological characteristics to capture these behaviors. On the contrary, for the intermediate dryness–wetness condition, M might have been overestimated, resulting in overestimation of λE. The overestimation of λE through PMBL in the FLUXNET mainly stemmed from the Howland, Niwot Ridge, Morgan Monroe, Tonzi Ranch (Fig. 6d), Tumbarumba (Fig. 6g), and Virginia Park sites (Table 5). This may again be because of violation of assumption of equilibrium between M and the relative soil moisture in these sites, particularly during the dry-down phase. This also points to the importance and necessity of including the radiometric surface temperature in the terrestrial evapotranspiration modeling to capture the surface moisture controls on λE.

The intersite variability of λE over all the SMEX-02 corn sites was quite consistent between measurements (Su et al. 2005; Prueger et al. 2005), but disparities between measurements for soybeans (e.g., in WC13) were also reported between site locations (Su et al. 2005; Prueger et al. 2005). This might also have affected the overall accuracy of the proposed approach. There are reports of systematic overestimation of R_N (20%; Kustas et al. 1998) and underestimation of λE (20%–25%; Wilson et al. 2002) in the eddy covariance measurements. Even if there is no error in R_N and λE measurements, the λE evaluation between the PMBL and tower would change by a small amount, leading to little or no net change in the overall evaluation for λE (since we have closed the surface energy balance). However, for better accuracy of such a modeling approach, the forcing state variables need to be more quality controlled. This is even more crucial at high-frequency temporal scales, where the probabilities of losing fluxes are at a maximum (Foken et al. 2004; Massman and Lee 2002; Moncrieff et al. 1997). One of the reasons for the relatively better accuracy of PMBL over the tropics and FLUXNET is because many random noises get filtered out in the monthly averaging.

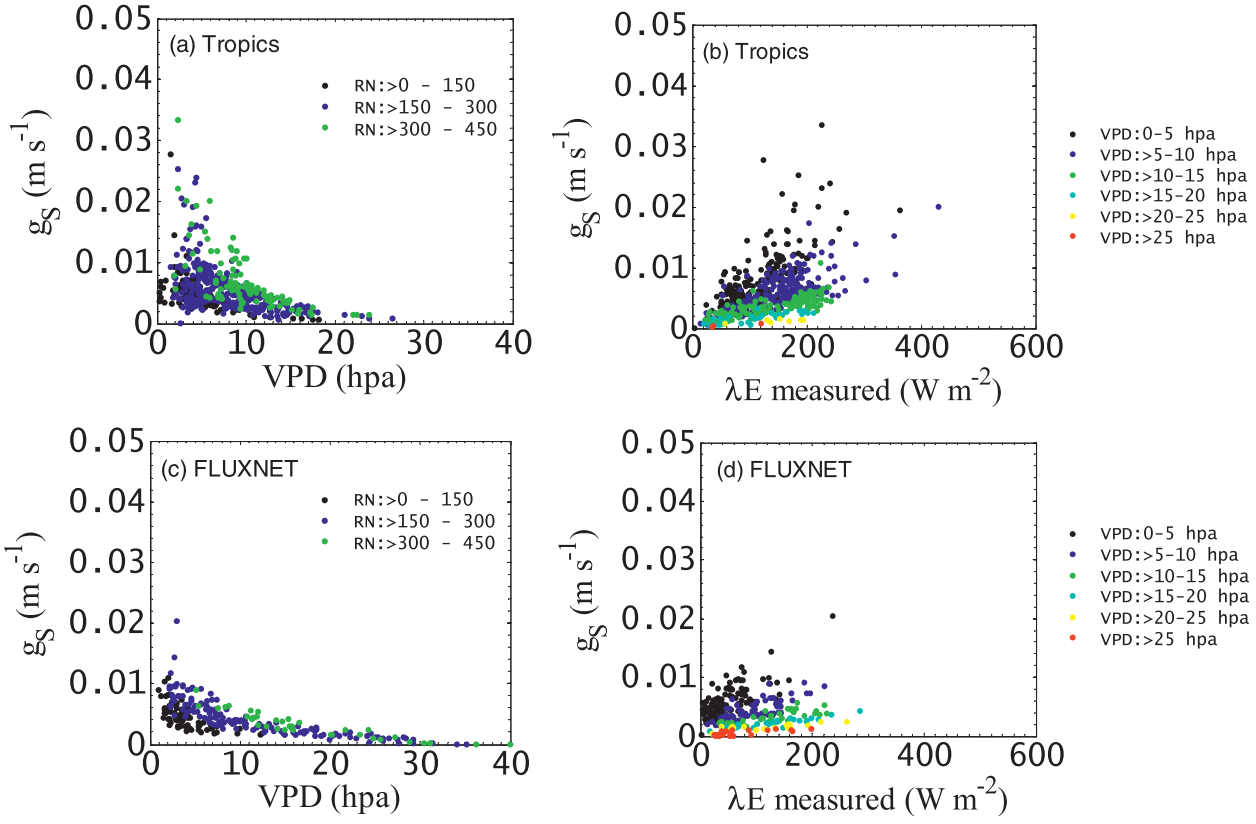

FIG. 10. Dependence of g_S in relation to (a) VPD for different levels of R_N over the tropics, (b) λE for different levels of evaporative demand (VPD) over the tropics, (c) VPD for different levels of R_N over FLUXNET, and (d) λE for different levels of evaporative demand (VPD) over FLUXNET.

From the tropical sites and the periods of analysis, it is evident that R_N is the prime driver of λE over the equatorial rain forests, and λE utilized approximately 65%–70% of R_N. This finding is consistent with the findings from field observations throughout the Amazonian rain forest (Malhi et al. 2002; Fisher et al. 2009). Among the two poorly validated tropical sites [LAS and Santarem KM77 (KM77)], KM77 experienced severe anthropogenic disturbances due to the biomass burning during this period (Fisher et al. 2009). This might have reduced the observed λE magnitude. Since no impact was found in the driving variables (R_N, G, T_a, and RH), PMBL was unable to track down these sudden falls in λE and produce significantly high RMSE. Clearly, in a majority of the cases, a close correspondence in λE estimates was found from both PMBL and PT-JPL, but they differ in some cases. Despite sharing the common moisture scalar equation ($M = \mathrm{RH}^{\mathrm{VPD}}$) with PT-JPL, PMBL uses only radiation and meteorological variables for estimating λE, while PT-JPL uses reflectance information to parameterize plant moisture constraint and other scalars. Such differences might have led to the disagreement between the two approaches in the La Selva site.

Sensitivity analysis clearly shows R_N to be the most important variable. All the observations in the present analysis used an all-wave net radiometer, which has typical uncertainties of ±10%. However, use of four component net radiometers might help reduce some errors in future studies.

The scatters between g_S versus λE and g_S versus VPD from all the datasets (Figs. 8–10) provided convincing evidence about the environmental response of stomata. The estimates of g_S are dependent on VPD; however, we have not specified g_S to behave exponentially with VPD. Still, g_S revealed the exponential behavior when linked with VPD, which is a classic pattern. This highlights the fidelity of the analytical approach. Linking g_S with independently measured λE revealed a distinct linearity between the two, and the slope of the linearity varies with the VPD. This is another theoretical finding of Monteith and indicates that our retrieval is consistent. An earlier hypothesis of Monteith (1995) showed that g_S decreases linearly with λE when VPD changes (with an inverse hyperbolic relation). The change in g_S is dominated by an increase in net energy input, but this change is partially offset by an increase in λE rate. After the net

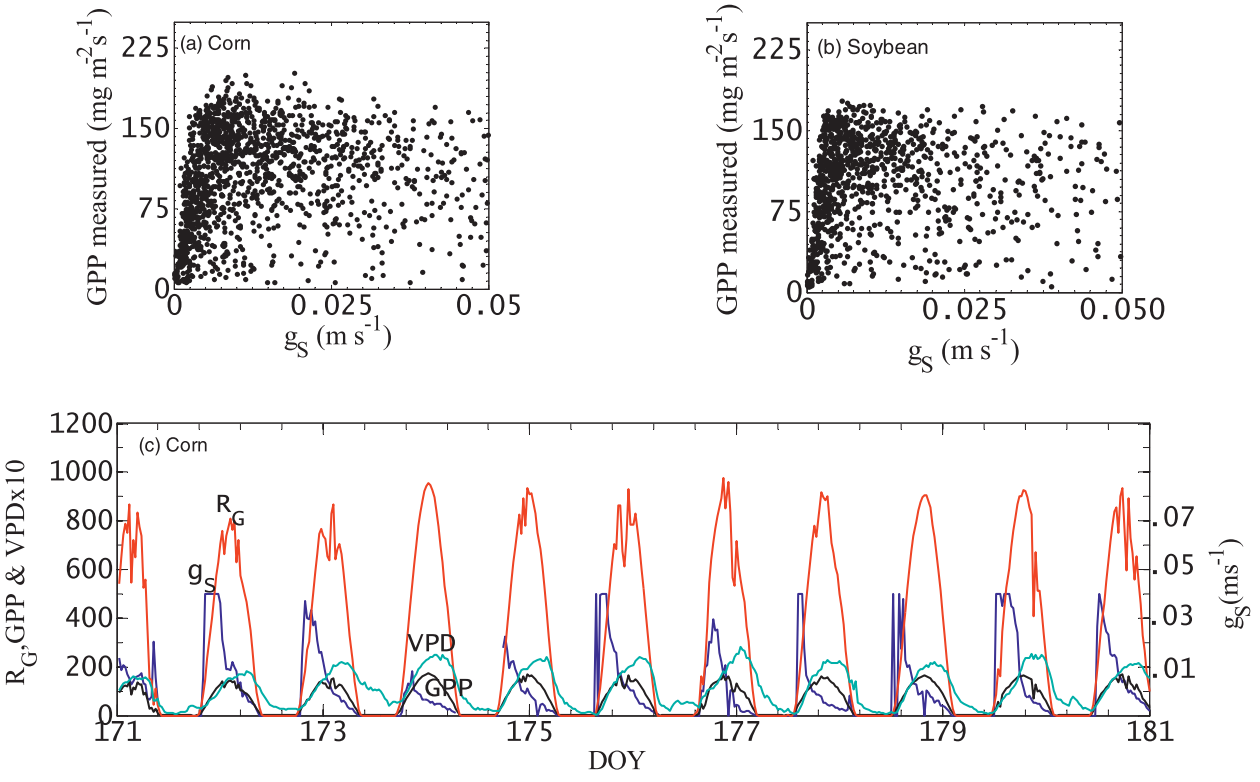

FIG. 11. Dependence of g_S on GPP for (a) corn and (b) soybeans during SMEX-02. (c) Illustrative example of the diurnal course of g_S (blue line) with GPP (black line, mg m^{-2} s^{-1}), R_G (W m^{-2}, red line), and VPD (hPa, green line).

energy input in the system exceeds a certain threshold, g_S starts decreasing even if λE increases. This supports the hypothesis that the stomata responds to VPD through a "feedback" mechanism based on the effect of λE on water potential gradient between the guard cells (Monteith 1995; Jones 1998). This is also the reason g_S typically peaks before noon and there is partial shutdown of stomata during the afternoon (Kramer and Boyer 1995).

The control of soil moisture to transpiration also became evident from the scatter between g_S and λE for different VPD levels. This supports the findings of Denmead and Shaw (1962), who hypothesized reduced stomatal conductance and stomatal closure at higher levels of soil moisture (high λE as well) when the atmospheric demand of water vapor increases (high VPD). This is apparent because the moisture content in the immediate vicinity of the root depletes rapidly at high atmospheric demand. This decreases the soil conductivity, and the soil will not be able to supply water immediately.

The observed scatter between GPP and g_S supports the fact that, when the soil moisture is available, their relationship is approximately linear (Tuzet et al. 2003; Meinzer et al. 1997). This was evident from data points over the corn and soybeans during SMEX-02. However, there may be hysteresis in the relationship under limiting surface moisture conditions (Tuzet et al. 2003), as found in the scatter and from the temporal behavior of g_S and GPP (Fig. 11). Such kinds of scatters are common when all the environmental variables that control g_S covary under the variable dry–wet cycle and the spread in the scatter increases as the surface dries out.

The prediction accuracy of hourly and monthly λE from the proposed approach is comparable with the results reported using the similar datasets and over other

TABLE 6. Sensitivity of PMBL-derived λE to different core variable inputs.

Variables	Sample range	Error	Sensitivity
T_a	15°–20°C	±2°C	0.08
	20°–25°C	±2°C	0.06
	25°–30°C	±2°C	0.04
RH	60%–70%	±10%	0.12
	70%–80%	±10%	0.09
	80%–90%	±10%	0.07
R_N	400–500 W m^{-2}	±10%	0.22
	500–600 W m^{-2}	±10%	0.23
	600–700 W m^{-2}	±10%	0.24
G	100–110 W m^{-2}	±10%	−0.04
	110–120 W m^{-2}	±10%	−0.05
	120–130 W m^{-2}	±10%	−0.06

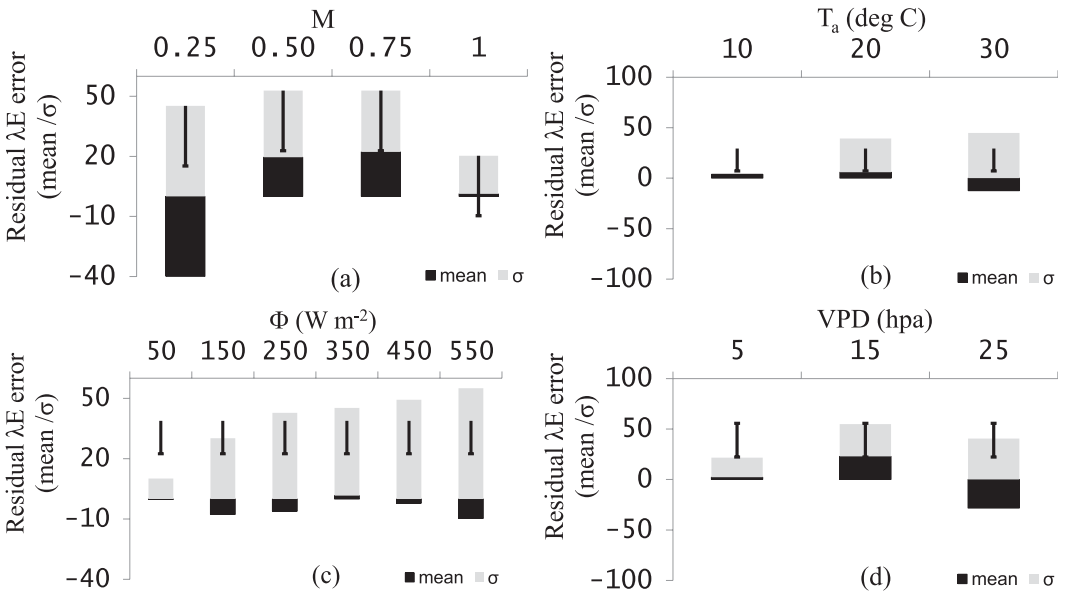

FIG. 12. Mean and standard deviation (σ) of the residual error in PMBL λE for various ranges of (a)–(d) M (RH^{VPD}), T_a, Φ, and VPD, respectively.

data in various regional and global studies based on the Priestley–Taylor and Penman–Monteith approaches. Over the agroecosystems, our results are also comparable with the one-source and two-source residual energy balance models. While estimating λE during the SMEX-02–SMACEX experiment, Su et al. (2005) obtained an RMSE of 47 W m^{-2} over corn and 40–48 W m^{-2} over soybeans using a single source λE model. Series of experimental results have been published based on the two source λE models (Mecikalski et al. 1999; Anderson et al. 2007, 2008), where the RMSE range varied between 37 and 66 W m^{-2} for hourly λE.

7. Summary and conclusions

We conclude that the combination of net available energy, air temperature, and vapor pressure deficit in the framework of Penman–Monteith, Priestley–Taylor, and Bouchet's complementary hypothesis showed significant promise for estimating λE when compared with independent observations of eddy covariance tower ground truth data. It provides a relatively better estimate than the Priestley–Taylor–based model over the tropics and a majority of the FLUXNET sites. The strength of this approach may be manifold: 1) it may be helpful to assess and test the land surface parameterization embedded in climate–Earth system models, and 2) in the developing countries of Southeast Asia and Africa, this method may offer a cost effective way for generating λE information from a network of automatic weather stations. The results also warrant further investigation, particularly into refinements in the representation of the surface wetness (or moisture). The results point to the use of radiometric surface temperature, which is a direct physical quantity in these regards and also a direct indicator of surface-to-root zone wetness (Norman et al. 1995; Kustas et al. 2005; Anderson et al. 2007). Where the method appears to work, this provides estimates of λE that would prove valuable in a range of applications. The ability to accurately predict stomatal conductance as a function of environmental variables would be useful in spatially explicit hydrology and climate modeling and predicting vegetation responses to global change.

The advent of Earth observation sciences may afford an opportunity to extend the PMBL methodology into the satellite platform by integrating the satellite R_N from Clouds and the Earth's Radiant Energy System (CERES) or Surface Radiation Budget (SRG), T_a and R_H from the Atmospheric Infrared Sounder (AIRS), and soil moisture from the Soil Moisture and Ocean Salinity Mission (SMOS) and the future Soil Moisture Active Passive (SMAP), thus allowing for more spatially explicit hydrological and physiological process studies.

Acknowledgments. We gratefully acknowledge NSIDC and CEOP for making the SMEX-02 and GCIP data available. K.M. acknowledges the comments from Dr. Bill Kustas, HRSL, USDA, and Dr. B. K. Bhattacharya, Space Applications Centre, India. We also acknowledge the site PIs of the tropical forest eddy covariance network

and FLUXNET network for the data permission. We acknowledge Dr. John Prueger for permitting us to use the SMEX-02. K.M. also acknowledges Dr. Junhak Lee for his help in map preparation and the postdoctoral research fellowship from the Jet Propulsion Laboratory's Research and Technology Development Climate Strategic Initiative. D.N. benefited in part through NSF CAREER (AGS-0847472, Anjuli Bamzai), USDA NIFA 2011-68002-30220, and NSF INTEROP OCI 0753116. KM was partly funded by the Natural Environment Research Council, United Kingdom, Grant NEE0191531. Three anonymous reviewers are also acknowledged for their helpful comments. The research was carried out at the Jet Propulsion Laboratory, California Institute of Technology, under a contract with the National Aeronautics and Space Administration.

REFERENCES

Anderson, M. C., J. M. Norman, J. R. Mecikalski, J. A. Otkin, and W. P. Kustas, 2007: A climatological study of evapotranspiration and moisture stress across the continental United States based on thermal remote sensing. 1: Model formulation. *J. Geophys. Res.,* **112,** D10117, doi:10.1029/2006JD007506.

——, ——, W. P. Kustas, R. Houborg, P. J. Starks, and N. Agam, 2008: A thermal-based remote sensing technique for routine mapping of land-surface carbon, water and energy fluxes from field to regional scales. *Remote Sens. Environ.,* **112,** 4227–4241.

Baldocchi, D. D., and Coauthors, 2001: FLUXNET: A new tool to study the temporal and spatial variability of ecosystem-scale carbon dioxide, water vapor, and energy flux densities. *Bull. Amer. Meteor. Soc.,* **82,** 2415–2434.

Ball, J. T., I. E. Woodrow, and J. A. Berry, 1987: A model predicting stomatal conductance and its contribution to the control of photosynthesis under different environmental conditions. *Progress in Photosynthesis Research,* J. Biggins, Ed., M. Nijhoff Publishers, 5.221–5.224.

Barr, A. G., K. Morgenstern, T. A. Black, J. H. McCaughey, and Z. Nesic, 2006: Surface energy balance closure by the eddy covariance method above three boreal forest stands and implications for the measurement of the CO_2 flux. *Agric. For. Meteor.,* **140,** 322–337.

Boegh, E., and H. Soegaard, 2004: Remote sensing based estimation of evapotranspiration rates. *Int. J. Remote Sens.,* **25,** 2535–2551.

——, ——, and A. Thomsen, 2002: Evaluating evapotranspiration rates and surface conditions using Landsat TM to estimate atmospheric resistance and surface resistance. *Remote Sens. Environ.,* **79,** 329–343.

Bonan, G. B., 1995: Land atmosphere CO_2 exchange simulated by a land-surface process model coupled to an atmospheric general circulation model. *J. Geophys. Res.,* **100,** 2817–2831.

——, 2008: Forests and climate change: Forcings, feedbacks, and the climate benefits of forests. *Science,* **320,** 1444–1449, doi:10.1126/science.1155121.

Bouchet, R. J., 1963: Evapotranspiration re'elle evapotranspiration potentielle, signification climatique. *Int. Assoc. Sci. Hydrol.,* **62,** 134–142.

Bowen, I. S., 1926: The ratio of heat losses by conduction and by evaporation from any water surface. *Phys. Rev.,* **27,** 779–787.

Brutsaert, W., and H. Stricker, 1979: An advection–aridity approach to estimate actual regional evapotranspiration. *Water Resour. Res.,* **15,** 443–450.

Budyko, M. I., N. A. Efimova, L. I. Zubenok, and L. A. Strokina, 1962: The heat balance of the earth's surface. *Izv. Akad. Nauk SSSR, Ser. Geogr.,* **1,** 6–16.

Cahill, A. T., M. B. Parlange, T. J. Jackson, P. O'Neill, and T. Schmugge, 1999: Evaporation from nonvegetated surface: Surface aridity methods and passive microwave remote sensing. *J. Appl. Meteor.,* **38,** 1346–1351.

Choudhury, B. J., R. J. Reginato, and S. B. Idso, 1986: An analysis of infrared temperature observations over wheat and calculation of latent heat flux. *Agric. For. Meteor.,* **37,** 75–88.

Denmead, O. T., and R. H. Shaw, 1962: Availability of soil water to plants as affected by soil moisture content and meteorological conditions. *Agron. J.,* **54,** 385–390.

Fisher, J. B., K. P. Tu, and D. D. Baldocchi, 2008: Global estimates of the land–atmosphere water flux based on monthly AVHRR and ISLSCP-II data, validated at 16 FLUXNET sites. *Remote Sens. Environ.,* **112,** 901–919.

——, and Coauthors, 2009: The land–atmosphere water flux in the tropics. *Global Change Biol.,* **15,** 2694–2714.

Foken, T., M. Goeke, M. Mauder, L. Mahrt, B. Amiro, and W. Munger, 2004: Post-field data quality control. *Handbook of Micrometeorology: A Guide for Surface Flux Measurements and Analysis,* X. Lee, W. J. Massman, and B. E. Law, Eds., Kluwer Academic Publishers, 181–203.

Foley, J. A., I. C. Prentice, N. Ramunkutty, S. Levis, D. Pollard, S. Sitch, and A. Haxeltine, 1996: An integrated biosphere model of land surface processes, terrestrial carbon balance, and vegetation dynamics. *Global Biogeochem. Cycles,* **10,** 603–628.

Jarvis, P. G., 1976: The interpretation the variations of leaf water potential and stomatal conductance found in canopies in the field. *Philos. Trans. Roy. Soc. London,* **B273,** 593–610.

——, and K. G. McNaughton, 1986: Stomatal control of transpiration: Scaling up from leaf to region. *Adv. Ecol. Res.,* **15,** 1–49.

Jones, H. G., 1998: Stomatal control of photosynthesis and transpiration. *J. Exp. Bot.,* **49,** 387–398.

Katul, G. G., S. Manzoni, S. Palmroth, and R. Oren, 2010: A stomatal optimization theory to describe the effects of atmospheric CO_2 on leaf photosynthesis and transpiration. *Ann. Bot.,* **105,** 431–442.

Kondo, J., N. Saigusa, and T. Sato, 1990: A parameterization of evaporation from bare soil surface. *J. Appl. Meteor.,* **29,** 385–389.

Kramer, P. J., and J. S. Boyer, 1995: *Water Relation of Plants and Soils.* Academic Press, 495 pp.

Kustas, W. P., J. H. Prueger, L. E. Hipps, J. L. Hatfield, and D. Meek, 1998: Inconsistencies in net radiation estimates from use of several models of instruments in a desert environment. *Agric. For. Meteor.,* **90,** 257–263.

——, J. L. Hatfield, and J. H. Prueger, 2005: The Soil Moisture–Atmosphere Coupling Experiment (SMACEX): Background, hydrometeorological conditions, and preliminary findings. *J. Hydrometeor.,* **6,** 791–804.

Lee, T. J., and R. Pielke, 1992: Estimating the soil surface specific humidity. *J. Appl. Meteor.,* **31,** 480–484.

Leuning, R., 1995: A critical appraisal of a combined stomatal–photosynthesis model for C_3 plants. *Plant Cell Environ.,* **18,** 339–355.

Lhomme, J. P., 1997: A theoretical basis for the Priestley–Taylor coefficient. *Bound.-Layer Meteor.,* **82,** 179–191.

——, A. Chehbouni, and B. Monteny, 2000: Sensible heat flux–radiometric surface temperature relationship over sparse vegetation: Parameterizing B^{-1}. *Bound.-Layer Meteor.,* **97,** 431–457.

Lohmann, D., E. Raschke, B. Nijssen, and D. Lettenmaier, 1998: Regional scale hydrology: I. Formulation of the VIC-2L model coupled to a routing model. *Hydrol. Sci. J.,* **43,** 131–141.

Malhi, Y., E. Pegoraro, A. D. Nobre, M. G. P. Pereira, J. Grace, A. D. Culf, and R. Clement, 2002: Energy and water dynamics of a central Amazonian rain forest. *J. Geophys. Res.,* **107,** 8061, doi:10.1029/2001JD000623.

Mallick, K., B. K. Bhattacharya, and N. K. Patel, 2009: Estimating volumetric surface moisture content for cropped soils using a soil wetness index based on surface temperature and NDVI. *Agric. For. Meteor.,* **149,** 1327–1342.

Massman, W. J., and X. Lee, 2002: Eddy covariance flux corrections and uncertainties in long-term studies of carbon and energy exchanges. *Agric. For. Meteor.,* **113,** 121–144.

Mecikalski, J. R., G. R. Diak, M. C. Anderson, and J. M. Norman, 1999: Estimating fluxes on continental scales using remotely sensed data in an atmospheric–land exchange model. *J. Appl. Meteor.,* **38,** 1352–1369.

Meinzer, F. C., T. M. Hinckley, and R. Ceulemans, 1997: Apparent responses of stomata to transpiration and humidity in a hybrid poplar canopy. *Plant Cell Environ.,* **20,** 1301–1308.

Moncrieff, J. B., and Coauthors, 1997: A system to measure surface fluxes of momentum, sensible heat, water vapour and carbon dioxide. *J. Hydrol.,* **188–189,** 589–611.

Monteith, J. L., 1965: Evaporation and environment. *The State and Movement of Water in Living Organisms,* G. E. Fogg, Ed., Symposia of the Society for Experimental Biology, Vol. 19, Academic Press, 205–234.

——, 1995: Accommodation between transpiring vegetation and the convective boundary layer. *J. Hydrol.,* **166,** 251–263.

Nappo, C. J., Jr., 1975: Parameterization of surface moisture and evaporation rate in a planetary boundary layer model. *J. Appl. Meteor.,* **14,** 289–296.

National Research Council, 1998: *GCIP Global Energy and Water Cycle Experiment (GEWEX) Continental-Scale International Project: A Review of Progress and Opportunities.* National Academies Press, 112 pp.

Niyogi, D., and S. Raman, 1997: Comparison of four different stomatal resistance schemes using FIFE observations. *J. Appl. Meteor.,* **36,** 903–917.

——, and Y. Xue, 2006: Soil moisture regulates the biological response of elevated atmospheric CO_2 concentrations in a coupled atmosphere biosphere model. *Global Planet. Change,* **54,** 94–108.

——, S. Raman, and K. Alapaty, 1998: Comparison of four different stomatal resistance schemes using FIFE observations. Part II: Analysis of terrestrial biospheric–atmospheric interactions. *J. Appl. Meteor.,* **37,** 1301–1320.

——, ——, and ——, 1999: Uncertainty in specification of surface characteristics, Part II: Hierarchy of interaction-explicit statistical analysis. *Bound.-Layer Meteor.,* **91,** 341–366.

——, K. Alapaty, S. Raman, and F. Chen, 2009: Development and evaluation of a coupled photosynthesis-based gas exchange evapotranspiration model (GEM) for mesoscale weather forecasting applications. *J. Appl. Meteor. Climatol.,* **48,** 349–368.

Noilhan, J., and S. Planton, 1989: A simple parameterization of land surface processes for meteorological models. *Mon. Wea. Rev.,* **117,** 536–549.

Norman, J. M., and G. S. Campbell, 1998: *An Introduction to Environmental Biophysics.* 2nd ed. Springer, 68 pp.

——, W. P. Kustas, and K. S. Humes, 1995: Source approach for estimating soil and vegetation energy fluxes in observations of directional radiometric surface temperature. *Agric. For. Meteor.,* **77,** 263–293.

Numaguti, A., 1993: Dynamics and energy balance of the Hadley circulation and the tropical precipitation zones: Significance of the distribution of evaporation. *J. Atmos. Sci.,* **50,** 1874–1887.

Paw U, K. T., and W. Gao, 1988: Applications of solutions to non-linear energy budget equations. *Agric. For. Meteor.,* **43,** 121–145.

Penman, H. L., 1948: Natural evaporation from open water, bare soil, and grass. *Proc. Roy. Soc. London,* **A193,** 120–146.

Pielke, R. A., Sr., and Coauthors, 2011: Land use/land cover changes and climate: Modeling analysis and observational evidence. *Wiley Interdiscip. Rev.: Climate Change,* **2,** 828–850, doi:10.1002/wcc.144.

Pitman, A., 2003: The evolution of, and revolution in, land surface schemes designed for climate models. *Int. J. Climatol.,* **23,** 479–510.

Priestley, C. H. B., and R. J. Taylor, 1972: On the assessment of surface heat flux and evaporation using large-scale parameters. *Mon. Wea. Rev.,* **100,** 81–92.

Prueger, J. H., and Coauthors, 2005: Tower and aircraft eddy covariance measurements of water, energy, and carbon dioxide fluxes during SMACEX. *J. Hydrometeor.,* **6,** 954–960.

Ramirez, J. A., M. T. Hobbins, and T. C. Brown, 2005: Observational evidence of the complementary relationship in regional evaporation lends strong support for Bouchet's hypothesis. *Geophys. Res. Lett.,* **32,** L15401, doi:10.1029/2005GL023549.

Roderick, M. L., and G. D. Farquhar, 2004: Changes in Australian pan evaporation from 1970 to 2002. *Int. J. Climatol.,* **25,** 1077–1090.

Sanchez, J. M., V. Caselles, R. Nicols, C. Coll, and W. P. Kustas, 2009: Estimating energy balance fluxes above a boreal forest from radiometric surface temperature observations. *Agric. For. Meteor.,* **149,** 1037–1049.

Sellers, P. J., and Coauthors, 1997: Modeling the exchanges of energy, water, and carbon between continents and the atmosphere. *Science,* **275,** 502–509.

Shuttleworth, W. J., R. J. Gurney, A. Y. Hsu, and J. P. Ormsby, 1989: FIFE: The variation in energy partition at surface flux sites. *Remote Sensing and Large Scale Processes,* A. Rango, Ed., IAHS Publ. 186, 67–74.

Stewart, J. B., and A. S. Thom, 1973: Energy budget in pine forest. *Quart. J. Roy. Meteor. Soc.,* **99,** 154–170.

Su, H., M. F. McCabe, E. F. Wood, Z. Su, and J. H. Prueger, 2005: Modeling evapotranspiration during SMACEX: Comparing two approaches for local- and regional-scale prediction. *J. Hydrometeor.,* **6,** 910–922.

Sugita, M., J. Usui, I. Tamagawa, and I. Kaihotsu, 2001: Complementary relationship with convective boundary layer model to estimate regional evaporation. *Water Resour. Res.,* **37,** 353–365.

Sumner, D. M., and J. M. Jacobs, 2005: Utility of Penman–Monteith, Priestley–Taylor, reference evapotranspiration, and pan evaporation methods to estimate pasture evapotranspiration. *J. Hydrol.,* **308,** 81–104.

Thom, A. S., 1975: Momentum, mass and heat exchange of plant communities. *Vegetation and the Atmosphere,* J. L. Monteith, Ed., Academic Press, 57–109.

Tobin, D. C., and Coauthors, 2006: Atmospheric Radiation Measurement site atmospheric state best estimates for Atmospheric Infrared Sounder temperature and water vapor retrieval validation. *J. Geophys. Res.,* **111,** D09S14, doi:10.1029/2005JD006103.

Trenberth, K. E., J. M. Caron, D. P. Stepaniak, and S. Worley, 2002: Evolution of El Niño–Southern Oscillation and global atmospheric surface temperatures. *J. Geophys. Res.,* **107,** 4065, doi:10.1029/2000JD000298.

Troufleau, D., J. P. Lhomme, B. Monteny, and A. Vidal, 1997: Sensible heat flux and radiometric surface temperature over sparse Sahelian vegetation. I. An experimental analysis of kB^{-1} parameter. *J. Hydrol.,* **188–189,** 815–838.

Tuzet, A., A. Perrier, and R. Leuning, 2003: A coupled model of stomatal conductance, photosynthesis and transpiration. *Plant Cell Environ.,* **26,** 1097–1116.

Werth, D., and R. Avissar, 2004: The regional evapotranspiration of the Amazon. *J. Hydrometeor.,* **5,** 100–109.

Wetzel, P. J., D. Atlas, and R. H. Woodward, 1984: Determining soil moisture from geosynchronous satellite infrared data: A feasibility study. *J. Climate Appl. Meteor.,* **23,** 376–391.

Wilson, K. B., and Coauthors, 2002: Energy balance closure at FLUXNET sites. *Agric. For. Meteor.,* **113,** 223–243.

Ye, Z., and R. Pielke, 1993: Atmospheric parameterization of evaporation from non–plant-covered surfaces. *J. Appl. Meteor.,* **32,** 1248–1258.